The Astrophysical Journal, 724:835–854, 2010 December 1
doi:10.1088/0004-637X/724/2/835

THE *SPITZER* c2d SURVEY OF WEAK-LINE T TAURI STARS. III. THE TRANSITION FROM PRIMORDIAL DISKS TO DEBRIS DISKS

Zahed Wahhaj[1], Lucas Cieza[1], David W. Koerner[2], Karl R. Stapelfeldt[3], Deborah L. Padgett[4], April Case[2], James R. Keller[5], Bruno Merín[6], Neal J. Evans II[7], Paul Harvey[7], Anneila Sargent[8], Ewine F. van Dishoeck[9], Lori Allen[10], Geoff Blake[11], Tim Brooke[4], Nicholas Chapman[3], Lee Mundy[12], and Philip C. Myers[13]
[1] Institute for Astronomy, University of Hawaii, Honolulu, HI 96814, USA
[2] Northern Arizona University, Building 19, Rm. 209, Flagstaff, AZ 86011-6010, USA
[3] Jet Propulsion Laboratory, California Institute of Technology, MS 183-900, 4800 Oak Grove Drive, Pasadena, CA 91109, USA
[4] Spitzer Science Center, California Institute of Technology, Mail Code 220-6, Pasadena, CA 91125, USA
[5] Department of Physics, 301 Weniger Hall, Oregon State University, Corvallis, OR 97331-6507, USA
[6] Herschel Science Centre, European Space Astronomy Centre (ESA), P.O. Box 78, 28691 Villanueva de la Cañada (Madrid), Spain
[7] Astronomy Department, University of Texas, 1 University Station C1400, Austin, TX 78712, USA
[8] Division of Physics, Mathematics, and Astronomy, California Institute of Technology, MS 105-24, Pasadena, CA 91125, USA
[9] Leiden Observatory, Postbus 9513, 2300 R.A. Leiden, The Netherlands
[10] National Optical Astronomy Observatory, 950 North Cherry Avenue, Tucson, AZ 85719, USA
[11] Division of Geological & Planetary Sciences, California Institute of Technology, MS 150-21, Pasadena, CA 91125, USA
[12] Astronomy Department, University of Maryland, College Park, MD 20742, USA
[13] Smithsonian Astrophysical Observatory, Harvard-Smithsonian Center for Astrophysics, 60 Garden Street, MS 42, Cambridge, MA 02138, USA
Received 2008 November 3; accepted 2010 September 21; published 2010 November 9

ABSTRACT

We present 3.6 to 70 μm *Spitzer* photometry of 154 weak-line T Tauri stars (WTTSs) in the Chamaeleon, Lupus, Ophiuchus, and Taurus star formation regions, all of which are within 200 pc of the Sun. For a comparative study, we also include 33 classical T Tauri stars which are located in the same star-forming regions. *Spitzer* sensitivities allow us to robustly detect the photosphere in the IRAC bands (3.6 to 8 μm) and the 24 μm MIPS band. In the 70 μm MIPS band, we are able to detect dust emission brighter than roughly 40 times the photosphere. These observations represent the most sensitive WTTSs survey in the mid- to far-infrared to date and reveal the frequency of outer disks ($r = 3$–50 AU) around WTTSs. The 70 μm photometry for half the c2d WTTSs sample (the on-cloud objects), which were not included in the earlier papers in this series, those of Padgett et al. and Cieza et al., are presented here for the first time. We find a disk frequency of 19% for on-cloud WTTSs, but just 5% for off-cloud WTTSs, similar to the value reported in the earlier works. WTTSs exhibit spectral energy distributions that are quite diverse, spanning the range from optically thick to optically thin disks. Most disks become more tenuous than $L_{\rm disk}/L_* = 2 \times 10^{-3}$ in 2 Myr and more tenuous than $L_{\rm disk}/L_* = 5 \times 10^{-4}$ in 4 Myr.

Key words: infrared: stars – planetary systems – protoplanetary disks – stars: pre-main sequence

Online-only material: color figures

1. INTRODUCTION

Observational and theoretical studies are converging on the consensus that planet formation occurs in circumstellar disks within a few million years (Myr) of the central star's core formation. Beyond an age of 10 Myr, the primordial disks of dust and gas are no longer observable. The evolution of the disks during this short period when they are observable contains indispensable information about the universal prospects for planet formation. The nearest star-forming regions are over 120 pc away, and they harbor many hundreds of young stars. However, it is difficult to ascertain which stars are young cloud members and which are old field stars. Surveys for Hα emission identified very young stars (age ~few Myr) which are actively accreting disks. Young stars were also identified by high X-ray activity and strong lithium absorption (in late-type stars). Weak Hα emission weak-line T Tauri stars (WTTSs) are also thought to be young but their age distribution is wider than that of classical T Tauri stars (CTTSs). Their modern definition on the basis of spectral properties, which is explained below, was chosen to select non-accreting young stars. They are found in very young clusters and also in older off-cloud regions (Cieza et al. 2007; Padgett et al. 2006). Thus, their evolutionary status is quite uncertain. In this paper, we will address this question in terms of the spectral energy distributions (SEDs) of WTTS disks, and thus try to understand where WTTSs fit in the larger disk evolution picture.

Current theories are trying to explain what drives the dispersal of the circumstellar gas, what halts gas accretion, in what order the different parts of the dust disk disappears, and how all these processes affect planet formation. The mechanisms proposed as pathways for disk dissipation include viscous accretion (Hartmann et al. 1998; Hueso & Guillot 2005), grain growth (Dullemond & Dominik 2005), photo-evaporation (Clarke et al. 2001; Alexander et al. 2006), and dust sweeping by companions (Lin & Papaloizou 1979; Artymowicz & Lubow 1994), among others. The general strategy for sorting out the relative importance of these mechanisms has been to observe large numbers of systems with different multiplicities, SEDs, accretion rates, and ages and to try to find correlations and trends between these measures. Early on, it was found that some WTTSs had passive disks that could be detected in the submillimeter (Beckwith et al. 1990). Osterloh & Beckwith (1995) showed that WTTSs had discernibly smaller millimeter wave emission than CTTSs. The scheme for the identification of accreting disks based on EW($H\alpha$) went through some refinement over the years. Martín (1998) adjusted the CTTS/WTTS classification by EW($H\alpha$) according to spectral type. White & Basri (2003) suggested a further adjustment of this classification and also showed that requiring full widths at 10% height >270 km s^{-1}

of the $H\alpha$ line was a much preferred way of identifying accretion disk stars (CTTSs). Further refinements and higher resolution spectra helped robustly identify stars which were weak accretors but not WTTSs (Barrado y Navascués & Martín 2003; Gras-Velázquez & Ray 2005; Sicilia-Aguilar et al. 2006). Following these refinements, Andrews & Williams (2005) found that only 15% of WTTSs had submillimeter emission while 91% of CTTSs were detected in the submillimeter. This signaled that most WTTSs had lost the small dust grains and pebbles in their outer disks ($r > 50$ AU) where most of the dust mass in primordial disks is usually found.

Before *Spitzer*, disk surveys performed at wavelengths longward of the *L* band provided an incomplete picture, as cool dust disks could remain undetected in regions beyond a few tens of AUs from the stars. Haisch et al. (2001) reported on *L* band excess rates in clusters and clouds from 0.3 to 30 Myr, showing a well behaved decline with cluster age. Excess rates were found to be 85% at 0.3 Myr (Meyer 1996), 52% at 3.2 Myr (Palla & Stahler 2000), and only 3% at 30 Myr (Barkhatova et al. 1985). With *Spitzer*'s dramatic improvement in sensitivity in the mid- and far-infrared, the dust out to several tens of AU can be detected in the nearby star-forming regions. There have been several *Spitzer* studies for disks around young stars, and they can be categorized as: disk surveys in clusters/associations, volume-limited debris disk surveys (often age selected) and star-forming region surveys. A plethora of *Spitzer* studies on clusters and moving groups have been conducted recently. Gutermuth et al. (2007) recently reported on an Infrared Array Camera (IRAC) and Multiband Imaging Photometer (MIPS) survey of NGC 1333 ($d = 300$ pc) showing the extremely high excess rate of 83%. An IRAC study of 2–3 Myr old IC 348 cluster in the Perseus cloud yielded an excess rate of 50%, while the WTTS excess rate was found to be 36% (Lada et al. 2006; Muench et al. 2007). Surveys of several middle aged groups like NGC 2362 (5 Myr), the η Chamaeleontis association (5–9 Myr), the Upper Sco-Cen OB association (5–20 Myr), and NGC 2547 (30 Myr) have yielded excess rates from 10% to 40% (Dahm & Hillenbrand 2007; Megeath et al. 2005; Chen et al. 2005; Carpenter et al. 2006; Hernández et al. 2006; Currie et al. 2007; Gorlova et al. 2007). Excess rates for older clusters like IC 2391 (50 Myr) and the Pleiades (100 Myr) are found to be around 25% (Gorlova et al. 2006; Stauffer et al. 2005; Siegler et al. 2007), but these are due to second generation debris disks. Despite the higher sensitivities attainable for the nearby associations like the Beta Pictoris Moving Group (12 Myr) and the TW Hydra association (8 Myr), their excess rates are found to be no higher than about 35% (Rebull et al. 2008; Low et al. 2005). In studies of young (1 Myr) molecular clouds, where membership has not been established for every member by spectroscopic indicators, only the number of stars with excess can be estimated. In *Spitzer* studies of the excess populations in Ophiuchus (Padgett et al. 2008) and Lupus (Chapman et al. 2007), it was found that 10%–30% were Class III, 40%–60% Class II, and the rest were less evolved. Alcalá et al. (2008) presented a *Spitzer* study of Chamaeleon II, where they found that the cloud has similar star-forming efficiencies to Taurus and Lupus, but a disk fraction that is much higher (70%–80%) than other star-forming regions.

The debris disk surveys generally attest to the fact that second generation dust disks are common in older systems (age >1 Gyr). In *Spitzer* studies of A stars, ranging 5–850 Myr in age, the mean excess rate is ∼30%. The maximum excess is found to be an inverse function of age, with a lifetimes of 150 Myr and 400 Myr at 24 μm and 70 μm, respectively (Rieke et al. 2005; Su et al. 2006). Much lower excess rates (10%–20%) have resulted from other main-sequence surveys (Silverstone et al. 2006; Meyer et al. 2007; Trilling et al. 2008). A surprising discovery was the high rates of infrared excess around main-sequence binary stars. The observed rates were 9% at 24 μm, 40% at 70 μm, and almost 60% when only considering very close binaries (separation <3 AU; Trilling et al. 2007).

One of the major goals of the *Spitzer* Cores to Disks (c2d) Legacy project (Evans et al. 2003) was to characterize the dust disks around WTTSs and find their place in the planet formation picture. Thus, 187 WTTSs/CTTSs in the nearest star-forming regions, Chamaeleon, Lupus, Ophiuchus, and Taurus were observed with IRAC at 3.6, 4.5, 5.8, and 8.0 μm and with MIPS at 24 and 70 μm. There have already been two publications on the preliminary data from these observations. We discuss these works in the next section.

2. OBSERVATIONS

2.1. Sample Selection

The sample for this survey is well described in Padgett et al. (2006), where photometry for about half the c2d WTTSs were presented. Basically, we attempted to select young stars with weak Hα emission for which the photosphere could be robustly detected at 24 μm. This meant we could only choose objects from the closer ($D < 200$ pc) star-forming clouds, Chamaeleon, Lupus, Ophiuchus, and Taurus. Young stars had been identified in these clouds by *ROSAT* detections of strong X-ray activity and by spectroscopic detections of Hα lines with small equivalent widths (EWs; generally less than 10 Å; Wichmann et al. 2000; Covino et al. 1997; Wichmann et al. 1999; Martín 1998). A further selection condition was that the objects exhibit lithium absorption stronger than a Pleiades star of the same spectral type. Thus, our sample should on average be younger than the Pleiades (100 Myr). Of course, lithium is only used as a reliable indicator of youth for spectral types later than G. Almost all of our stars are of spectral types K and M.

As mentioned earlier, preliminary results from these observations have already been presented in two earlier works. Padgett et al. (2006) studied the 83 c2d WTTSs that had both pointed IRAC and MIPS observations. Only a few of these deep pointed observations were inside the c2d scan maps of the five large clouds (Evans et al. 2003). The rest were off-cloud but still less than 6 deg away from the cloud boundaries in projected separation. These deeper off-cloud observations were made when the scan maps did not provide adequate sensitivity with respect to the target's photosphere. An excess rate of 6% was found for these objects. Cieza et al. (2007) collected all the known WTTSs that were located within the cloud maps, adding many targets in Perseus that were not in the original c2d WTTS sample. They found that ∼20% of the WTTSs covered by the cloud maps had excess emission from dust at 24 μm. Seventy micron photometry was not presented at that time. Here we present 3.6–70 μm data on the entire c2d WTTS sample, both on-cloud and off-cloud, thus revealing the nature of dust disks around WTTSs out to several tens of AU from the star. For half our sample we are sensitive to disks as tenuous as the debris disk β Pictoris ($L_{\rm disk}/L_* = 2 \times 10^{-3}$), while for the other half we are only sensitive to brighter disks.

Since the publication of the first two papers in this series, we have refined the CTTS/WTTS classification criteria according to White & Basri (2003), who required a full width at 10% of

$H\alpha$ line height (FW.1H($H\alpha$)) greater than 270 km s^{-1} (in high-resolution spectra) to classify a star as a CTTS. In the absence of high-resolution spectra, we use the EW($H\alpha$) to classify the objects. According to White & Basri (2003), we classify a star as CTT when EW($H\alpha$) >3 Å for spectral types earlier than K0, when EW($H\alpha$) > 10 Å for K7-M2.5, when EW($H\alpha$) > 20 Å for M2.5-M5 and when EW($H\alpha$) > 40 Å for later types. The idea is that for an M star, stellar activity alone can produce a line width of 10 Å (Martín 1998), whereas for earlier types the line is often saturated. We had available reduced high-resolution optical spectra (KPNO 4m, Echelle Spectra, $R \sim 42000$; Keller et al. 2003, Keller 2004) for 161 of our 187 targets. From these, we were able to measure the FW.1H($H\alpha$) to a precision of roughly 30 km s^{-1}. The measured line widths are presented in Table 1. Some of the targets which would have been classified as WTTSs in the earlier papers in this series are now classified as CTTSs, and thus old results are not directly comparable. Sixteen stars, which were originally classified as WTTS objects, are now reclassified as CTTSs. They are UX Tau, FX Tau, ZZ Tau, V710 Tau, V807 Tau, V836 Tau, Sz 41, RX J1150.4-7704, RX J1518.9-4050, Sz 65, Sz 96, RX J1608.5-3847, RX J1608.6-3922, ROX 16, SR 9, and ROX 39. Furthermore, two objects were reclassified as WTTSs from CTTSs and they are RX J1149.8-7850 and RX J1612.3-1909.

2.2. *Spitzer Photometry*

In the 50 *Spitzer* hours allotted to this program (PID, 173) we observed 154 WTTS objects and 33 CTTS. One-third of our WTTSs were in the denser clouds regions (with $A_v > 3$), one-third were between 0 deg and 3 deg from the cloud edge ($A_v = 3$ isoline), and one-third were between 3 deg and 6 deg from the cloud edge. Given the velocity dispersion of these cloud associated sources, stars originating in the clouds should travel no farther than 6 deg in 10 Myr (Hartmann et al. 1991). We obtained *Spitzer* photometry with its IRAC (Fazio et al. 2004) and MIPS (Rieke et al. 2004) instruments. The details of the observing parameters are well-described in Padgett et al. (2006), so we will just provide the basic template here. Two 12 s exposures, plus one short 0.6 exposure in "high dynamic range" mode were taken with IRAC. These were adequate to detect the photosphere with S/N > 50 in the four IRAC bands centered on 3.6, 4.5, 5.8 and 8.0 μm. At 24 μm, we attempted to detect the photosphere, with S/N > 20 which resulted in integration times between 42 and 420 s. At 70 μm, the photospheres are too faint to detect, and so we used the same exposure time of 360 s for all objects. This allows us to detect disks as faint as $f_{\rm lum}$ (or $L_{\rm disk}/L_*$) $= 10^{-3}$ for the brighter half of our sample, and disks as faint as $f_{\rm lum} = 10^{-2}$ for the other half. Photometry were obtained from the IRAC and MIPS maps using the c2d pipeline, as described in Harvey et al. (2006), Young et al. (2005), and the c2d data delivery document.

At 70 μm, aperture photometry was conducted on the filtered post-BCD (Basic Calibrated Data) images obtained from the Infrared Science Archive (IRSA; http://irsa.ipac.caltech.edu/). The images are super-sampled so that the pixels are of size 4″ instead of the original 10″. The aperture centers were fixed using the astrometry information in the FITS file headers. We used an aperture of radius 16″ and a sky annulus with inner and outer radii of 18″ and 39″, for which an aperture correction factor of 2.07 is recommended (MIPS data handbook, updated 2009 October). The IDL routine *APER.PRO* was used to perform the photometry and estimate the uncertainties which are obtained from the pixel-to-pixel noise in the sky annulus. Detections with signal-to-noise ratio (S/N) above 3 are initially considered real, but subsequently checked for shape, confusion with nearby, sources, and nearby nebulosity. Upper limits of 3σ, for sources not detected at 70 μm, are given in Table 2. The absolute calibration uncertainty for 70 μm is 15% (Gordon et al. 2007). This error is added in quadrature to the photometric uncertainty. We note that the 70 μm fluxes presented in this paper are larger by a factor of ∼2 than those reported in Padgett et al. (2006), as the earlier photometry was done before aperture radii and correction factors were properly calibrated and standardized by the Spitzer Science Center (http://ssc.spitzer.caltech.edu/mips/).

Because of the significantly lower imaging resolution at 70 μm, it is much more difficult to decide which detections are bona fide, compared to the other bands. This is especially true when the S/N of the detections are below 10, or when there is neighboring nebulosity. We consider any detected 70 μm emission to be associated with the target star with high confidence when the separation of the center of emission and the star as seen in the IRAC bands is less than $\mathrm{FWHM}_{70}/(\mathrm{S/N})_{70}$. Thus, for a 70 μm detection with an S/N of 3, the separation between the emission centers must be less than $16''/3 \sim 5''.3$. When the separation is larger than this limit, but less than the nominal FWHM at 70 μm (16″), we check in the IRAC images to see if the 70 μm emission center is better matched by any other source. If there is no better match, and the surrounding nebulosity at 24 μm and 70 μm can be ruled out as sources of confusion, then the emission is still assumed to be coming from the target star. Where the 70 μm detections suffer from confusion, it is possible that the 24 μm photometry, as given in the IRSA catalogs, are also contaminated. For these targets, the 24 μm aperture photometry was repeated (replacing the IRSA catalog values) according to the MIPS data handbook recommendations for an aperture radius of 7″. This resulted in new photometry for the WTTS sources RX J1607.2-3839, RX J1608.3-3843, and RX J1609.7-3854.

In Figure 1, we show all the WTTS 70 μm detections which we consider to be bona fide. Overlaid in the figure are contours from *Spitzer* maps in the 3.6, 8, and 24 μm bands. When a nearby source was detected close to the target aperture, it was subtracted using a custom IDL routine. This routine takes the centers of nearby sources and removes the median flux in annuli around this center. Adjacent sources were removed in the case of HBC 423, HBC 422, DI TAU, HV TAU, and RX J0445.8+1556 (see Figure 1). A bar-like artifact also had to be removed in the case of ROXS 43A. In some cases, the spurious detection is entirely due to a known source close to the target. We discuss these cases below. The flux detected in the DoAr 21 aperture probably originates from the bright H II region FG Oph 17 which reaches within 4″ of the target. In the *Spitzer* 8 and 24 μm images, we also see the surrounding nebulosity getting stronger at longer wavelengths. The 70 μm emission is also highly irregular in shape and it is difficult to claim with confidence that it results from disk emission. Jensen et al. (2009) detected polycyclic aromatic hydrocarbon (PAH) emission in an irregular distribution over hundreds of AU from the star but could not ascertain if there was any emission coming from a circumstellar disk. In the case of HV Tau, the 70 μm emission is actually coming from HV Tau C (Stapelfeldt et al. 2003), which is an edge-on disk that lies 4″ to NE of the target (the AB component). There is a very bright YSO, 2MASS J16272146-2441430, contaminating the field and causing a spurious detection for ROX 21. The RX J0445.8+1556 detection was because of contamination

Table 1
Stellar Properties

ID	Type	EW(H_α) (Å)	FW.1H (km s^{-1})	SpT	SED Type	Bin. Notes	Bin. Ref.	T_{eff} (K)	$L_\star$ ($L_\odot$)	Age (yr)	A_v (mag)	d_{edge} (deg)	L_d/L_*
NTTS032641+2420	WTTSs	0.00	0	K1	RJ	<0.2	9	5050	0.49	4.80E+07	0.1	3.6	<6.7E-04
NTTS040047+2603	WTTSs	−10.00	155	M2	RJ			3550	0.28	2.50E+06	0.1	2.2	<1.1E-03
RX J0405.3+2009	WTTSs	−1.80	−114	K1	RJ	<0.13	8	5050	2.14	7.70E+06	0.1	5.5	<1.5E-04
NTTS040234+2143	WTTSs	−6.60	–	M2	RJ			3550	0.18	4.50E+06	0.2	4.7	<2.1E-03
RX J0409.2+1716	WTTSs	−3.70	220	M1	RJ	<0.13	8	3700	0.49	1.80E+06	0.4	3.3	<6.6E-04
RX J0409.8+2446	WTTSs	−1.80	84	M1.5	RJ	<0.13	8	3700	0.39	2.40E+06	0.0	1.3	<1.0E-03
RX J0412.8+1937	WTTSs	−0.60	84	K6	RJ	<0.13	8	4200	0.50	7.70E+06	0.2	3.2	<1.1E-03
LkCa 1	WTTSs	−2.80	159	M4V	RJ	<0.13	1	3350	0.62	1.10E+06	0.7	−0.2	<6.1E-04
LkCa 3	WTTSs	−0.14	176	M1V	RJ	0.47	1	3700	2.22	4.20E+05	0.6	−0.2	<1.1E-04
LkCa 5	WTTSs	−2.50	160	M2V	RJ	<0.13	1	3550	0.45	1.60E+06	0.4	−0.4	<6.7E-04
NTTS041559+1716	WTTSs	−1.90	–	K7	RJ			4050	0.45	5.80E+06	0.1	1.8	<8.7E-04
LkCa 7	WTTSs	−0.53	133	K7V	RJ	1.05	1	4050	1.23	1.20E+06	0.7	−0.5	<2.8E-04
RX J0420.3+3123	WTTSs	−0.50	111	K4	RJ	<0.13	8	4550	0.39	2.80E+07	0.3	2.3	<1.2E-03
HD 283572	WTTSs	−0.63	−187	G2III	RJ	<0.13	1	5850	9.75	6.30E+06	0.8	0.1	<1.7E-05
LkCa 21	WTTSs	−5.50	155	M3...	RJ	<0.13	1	3450	0.77	8.60E+05	0.8	0.1	<6.3E-03
RX J0424.8+2643	WTTSs	−2.10	−125	K0	RJ			5250	3.51	6.30E+06	1.4	−0.4	<1.8E-04
NTTS042417+1744	WTTSs	1.60	−217	K1	RJ			5050	1.89	8.70E+06	0.7	0.8	<1.5E-04
DH Tau	CTTSs	−38.50	–	M0.5V:e	TNIR	<0.005	1;2	3850	1.77	6.70E+05	4.5	−0.4	3.30E-02
DI Tau	WTTSs	−2.00	128	M0.5V:e	RJ	0.12	1;2	3850	0.97	1.10E+06	0.6	−0.4	<1.2E-02
UX Tau	CTTSs	−0.67	503	G5V:e...	TNIR	<0.13	1	5750	6.69	7.90E+06	3.5	0.2	4.70E-02
FX Tau	CTTSs	−14.50	302	M4e	TNIR	0.91	1;2	3350	1.55	6.60E+04	3.3	−0.6	6.40E-02
ZZ Tau	CTTSs	−14.00	309	M3	TIRAC	0.029	1	3450	0.80	8.00E+05	1.0	−0.3	3.60E-02
V927 Tau	WTTSs	−10.00	–	M4	RJ	0.3	1;2	3350	0.52	1.30E+06	0.3	−0.5	<7.9E-04
NTTS042835+1700	WTTSs	−1.10	98	K5	RJ			4350	0.44	1.40E+07	0.4	0.9	<8.1E-04
V710 Tau	CTTSs	−3.87	313	K7	TNIR			4050	0.85	2.10E+06	0.7	0.3	1.00E-01
NTTS042916+1751	WTTSs	−0.56	114	K7	RJ			4050	0.70	2.80E+06	0.6	0.1	<4.9E-04
V928 Tau	WTTSs	−1.80	125	M...	RJ	0.18	1;2	3200	2.36	2.80E+04	9.5	−0.6	<1.2E-04
NTTS042950+1757	WTTSs	−1.07	114	K7	RJ			4050	0.46	5.60E+06	0.6	0.2	<7.4E-04
RX J0432.8+1735	WTTSs	−1.90	138	M2	T24	<0.13	8	3550	0.48	1.50E+06	0.7	0.5	3.70E-03
GH Tau	CTTSs	−27.50	480	M2e	TNIR	0.35	1	3550	1.83	1.10E+05	2.7	−0.3	5.50E-02
V807 Tau	CTTSs	−13.50	405	M...	TIRAC	0.41	2	3200	5.85	2.80E+04	8.1	−0.3	1.10E-02
V830 Tau	WTTSs	−1.80	–	K7	RJ	<0.13	1	4050	1.08	1.50E+06	0.9	−0.5	<3.6E-04
GK Tau	CTTSs	−30.50	344	K7	TNIR	12.2	1;2	4050	3.95	4.30E+05	5.0	−0.4	9.20E-02
WA Tau1	WTTSs	−0.60	122	K0IV	RJ	<0.13	1	5250	3.04	7.30E+06	0.2	−0.1	<1.3E-04
NTTS043230+1746	WTTSs	−9.00	−193	M2	RJ			3550	0.45	1.60E+06	0.6	0.9	<6.0E-04
RX J0435.9+2352	WTTSs	−6.27	143	M1.5	RJ	0.069	8	3700	0.68	1.30E+06	0.5	0.1	<6.6E-04
LkCa 14	WTTSs	−0.90	133	M0:V	RJ	<0.13	1	3850	0.79	1.30E+06	0.3	−0.8	<7.6E-04
RX J0437.4+1851	WTTSs	−1.10	111	K6	RJ			4200	0.86	3.20E+06	0.2	1.6	<5.3E-04
RX J0438.2+2023	WTTSs	−1.20	–	K2	RJ	0.464	8	4900	0.64	2.20E+07	0.5	2.4	<9.3E-04
HV Tau	WTTSs	−8.50	194	M1	T24	0.035	2	3700	1.80	5.10E+05	2.9	−0.8	3.8E-04
RX J0438.6+1546	WTTSs	−0.07	−65	K2	RJ			4900	1.74	6.80E+06	0.2	0.8	<2.3E-04
RX J0439.4+3332A	WTTSs	−0.07	100	K5	RJ	<0.13	8	4350	0.09	1.20E+08	1.8	0.0	<6.0E-03
IW Tau	WTTSs	−4.00	133	K7V	RJ	0.27	1;2	4050	1.29	1.20E+06	1.3	−0.7	<3.4E-04
ITG33	CTTSs	−53.00	–	M3	TNIR			3450	0.19	3.30E+06	10.4	−0.7	1.20E-01
HBC422	WTTSs	−1.92	94	K7	T70	0.3	1	4050	1.93	7.50E+05	4.8	−1.0	6.9E-03
HBC423	WTTSs	−1.38	77	M1	TNIR	0.33	1	3700	2.43	3.70E+05	6.1	−1.0	8.2E-02
RX J0445.8+1556	WTTSs	0.93	−320	G5	RJ			5750	5.80	9.00E+06	0.2	0.6	<7.7E-04
RX J0452.5+1730	WTTSs	−0.05	−23	K4	RJ	<0.13	8	4550	0.60	1.30E+07	0.2	1.2	<4.9E-04
RX J0452.8+1621	WTTSs	−0.95	144	K6	RJ	0.478	8	4200	1.28	1.70E+06	0.6	1.5	<3.3E-04
LkCa 19	WTTSs	−1.20	110	K0V	T24			5250	2.35	9.50E+06	0.8	0.1	2.50E-04
NTTS045251+3016	WTTSs	−1.40	77	K5	RJ	0.034	10	4350	1.60	2.00E+06	0.8	0.1	<3.0E-04
RX J0457.2+1524	WTTSs	−0.13	−114	K1	RJ	0.57	8	5050	2.93	5.50E+06	0.1	2.9	<1.4E-04
RX J0457.5+2014	WTTSs	−0.18	−96	K3	RJ	6.87	8	4700	1.09	8.90E+06	0.4	4.6	<4.8E-04
RX J0458.7+2046	WTTSs	0.00	−53	K7	RJ	6.11	8	4050	0.71	2.70E+06	0.3	4.4	<7.4E-04
RX J0459.7+1430	WTTSs	−0.01	57	K4	RJ	<0.13	8	4550	0.79	1.10E+07	0.2	4.1	<4.3E-04
V836 Tau	CTTSs	−7.70	240	K7V	TIRAC			4050	1.18	1.30E+06	3.4	−0.1	3.50E-02
RX J0842.4-8345	WTTSs	−1.00	171	K4	RJ	<0.13	6	4550	1.80	3.30E+06	1.1	7.4	<7.8E-04
RX J0848.0-7854	WTTSs	−5.57	210	M3.2Ve	RJ	<0.13	6	3450	1.13	4.50E+05	0.2	6.4	<2.2E-04
RX J0902.9-7759	WTTSs	−1.70	179	M3	RJ	<0.13	6	3450	0.52	1.30E+06	0.0	5.9	<9.8E-04
RX J0915.5-7609	WTTSs	−1.15	120	K6	RJ	0.111	6	4200	1.59	1.30E+06	0.7	5.5	<1.3E-03
RX J0935.0-7804	WTTSs	−4.90	117	M1	RJ	0.36	6	3700	0.84	1.10E+06	0.4	3.9	<4.4E-04
RX J0942.7-7726	WTTSs	−2.16	109	K8	RJ	<0.13	6	3950	0.59	2.90E+06	0.8	3.6	<7.4E-04
RX J1001.1-7913	WTTSs	−1.80	113	K8	RJ	<0.13	6	3950	0.72	2.10E+06	0.5	2.8	<5.4E-04
RX J1005.3-7749	WTTSs	−2.80	127	M1	RJ	<0.13	6	3700	0.85	1.10E+06	0.5	2.3	<4.3E-04
CS Cha	CTTSs	−54.30	395	M0	T24	2435 days	7	3850	1.73	6.70E+05	0.6	−0.5	1.40E-01

Table 1
(Continued)

ID	Type	EW(H_α) (Å)	FW.1H (km s^{-1})	SpT	SED Type	Bin. Notes	Bin. Ref.	T_{eff} (K)	$L_\star$ ($L_\odot$)	Age (yr)	A_v (mag)	d_{edge} (deg)	L_d/L_*
RX J1108.8-7519	WTTSs	−1.70	218	M2	RJ	0.15	6	3550	0.86	9.00E+05	0.5	1.1	<5.2E-04
Sz 30	WTTSs	−4.90	176	M0	RJ	1.24	3	3850	0.90	1.20E+06	0.9	−0.4	<7.0E-04
Sz 41	CTTSs	0.00	378	K0	TIRAC	1.97	3	5250	5.70	4.00E+06	4.0	0.0	2.10E-02
RX J1117.0-8028	WTTSs	−11.77	159	M2	RJ	<0.13	6	3550	0.72	1.00E+06	0.1	2.2	<3.3E-04
RX J1123.2-7924	WTTSs	−3.00	173	K8	RJ	<0.13	6	3950	0.11	4.20E+07	2.4	1.4	<3.9E-03
RX J1129.2-7546	WTTSs	−0.23	49	K3	RJ	0.534	6	4700	1.57	5.50E+06	1.6	1.3	<9.0E-04
RX J1149.8-7850	WTTSs	−32.00	120	M0	TNIR	<0.13	6	3850	1.38	7.70E+05	0.9	2.0	2.80E-01
RX J1150.4-7704	CTTSs	−1.70	388	K2	RJ	<0.13	6	4900	1.41	9.00E+06	0.7	1.9	<3.0E-04
T Cha	WTTSs	−2.70	−293	F5	TNIR			6400	45.88	9.20E+05	10.3	1.5	2.20E-02
RX J1158.5-7754	WTTSs	−0.50	120	K2	RJ	0.073	6	4900	6.21	1.70E+06	1.1	2.3	<6.3E-05
RX J1158.5-7913	WTTSs	−3.34	194	K3	RJ	<0.13	6	4700	2.14	3.70E+06	2.6	1.5	<2.5E-04
RX J1159.7-7601	WTTSs	−0.39	91	K2	RJ	<0.13	6	4900	2.75	4.10E+06	1.2	2.8	<4.3E-04
RX J1202.1-7853	WTTSs	−2.48	170	K7	RJ	<0.13	6	4050	1.81	8.00E+05	1.0	1.7	<2.1E-04
RX J1204.6-7731	WTTSs	−4.20	99	M3	RJ	<0.13	6	3450	0.72	9.80E+05	0.0	2.4	<6.0E-04
RX J1216.8-7753	WTTSs	−4.00	117	M4	RJ	<0.13	6	3350	0.51	1.30E+06	0.2	1.7	<7.8E-04
RX J1219.7-7403	WTTSs	−3.30	117	K8	RJ	<0.13	6	3950	1.02	1.30E+06	0.7	3.3	<3.5E-04
RX J1220.4-7407	WTTSs	−2.24	155	K7m...	RJ	0.296	6	4050	1.70	8.60E+05	0.9	3.2	<2.1E-04
RX J1239.4-7502	WTTSs	−0.07	137	K2	RJ	<0.13	6	4900	4.00	2.70E+06	0.1	1.8	<7.3E-05
RX J1301.0-7654	WTTSs	−3.90	−350	M0.5	RJ	<0.13	6	3850	1.92	6.40E+05	0.7	0.1	<2.7E-03
RX J1507.6-4603	WTTSs	−0.36	131	K2	RJ			4900	1.56	8.00E+06	0.5	5.5	<4.6E-04
RX J1508.6-4423	WTTSs	−0.55	−229	G8	RJ	not SB	7	5500	2.52	1.50E+07	0.0	7.1	<2.2E-04
RX J1511.6-3550	WTTSs	−0.14	143	K5	RJ			4350	0.96	4.20E+06	0.4	2.0	<5.6E-04
RX J1515.8-3331	WTTSs	−1.57	85	K0	RJ			5250	3.32	6.70E+06	0.0	2.2	<2.8E-04
RX J1515.9-4418	WTTSs	−1.03	117	K1	RJ	not SB	7	5050	1.23	1.50E+07	0.7	6.5	<4.9E-04
RX J1516.6-4406	WTTSs	0.00	−137	K2	RJ	not SB	7	4900	1.41	8.90E+06	0.4	6.7	<5.6E-04
RX J1518.9-4050	CTTSs	−1.37	914	G8	RJ			5500	3.30	1.10E+07	0.3	7.2	<2.3E-04
RX J1519.3-4056	WTTSs	−0.28	−504	K0	RJ			5250	2.38	9.70E+06	0.8	7.8	<3.0E-04
RX J1522.2-3959	WTTSs	−1.80	166	K3	RJ			4700	1.50	5.90E+06	0.9	4.5	<3.8E-04
RX J1523.4-4055	WTTSs	0.00	81	K2	RJ	not SB	7	4900	1.32	9.80E+06	0.4	6.6	<5.4E-04
RX J1523.5-3821	WTTSs	−5.93	302	M2	RJ	not SB	7	3550	0.56	1.30E+06	0.3	3.0	<9.1E-04
RX J1524.0-3209	WTTSs	−2.26	127	K7	RJ	3000 days	7	4050	1.62	9.10E+05	0.7	3.2	<3.3E-04
RX J1524.5-3652	WTTSs	−0.07	−50	K1	RJ	not SB	7	5050	1.88	8.70E+06	0.1	1.5	<3.2E-04
RX J1525.5-3613	WTTSs	−0.29	166	K2	RJ	not SB	7	4900	1.98	5.90E+06	0.5	1.0	<4.6E-04
RX J1525.6-3537	WTTSs	−1.56	170	K6	RJ	not SB	7	4200	1.28	1.70E+06	0.6	0.7	<4.5E-04
RX J1526.0-4501	WTTSs	−2.40	−159	G5	RJ	not SB	7	5750	2.64	1.50E+07	0.4	4.7	<2.5E-04
RX J1538.0-3807	WTTSs	−0.46	113	K5	RJ	not SB	7	4350	0.90	4.60E+06	0.2	3.2	<6.7E-04
RX J1538.6-3916	WTTSs	−0.12	80	K4	RJ	not SB	7	4550	1.67	3.60E+06	0.4	4.5	<3.8E-04
RX J1538.7-4411	WTTSs	0.00	−56	G5	RJ			5750	5.19	1.00E+07	0.7	3.4	<1.1E-04
Sz 65	CTTSs	−3.30	336	K8	TIRAC			3950	3.53	4.50E+05	2.6	−0.2	6.20E-02
RX J1540.7-3756	WTTSs	−0.49	145	K6	RJ	not SB	7	4200	1.00	2.50E+06	0.1	2.8	<6.5E-04
RX J1543.1-3920	WTTSs	−0.13	127	K6	RJ			4200	1.09	2.20E+06	0.1	3.9	<1.6E-03
RX J1546.7-3618	WTTSs	−0.57	127	K1	RJ			5050	2.27	7.10E+06	0.6	0.9	<2.8E-04
RX J1547.7-4018	WTTSs	−0.63	−99	K1	RJ			5050	2.42	6.70E+06	0.1	2.6	<3.4E-04
PZ99 J154920.9-2600	WTTSs	0.00	−123	K0	RJ			5250	2.18	1.10E+07	0.8	6.2	<8.8E-05
Sz 76	WTTSs	−10.30	227	M1	TIRAC			3700	0.38	2.40E+06	0.6	0.1	8.60E-02
RX J1550.0-3629	WTTSs	−0.06	−46	K2	RJ			4900	1.84	6.40E+06	0.2	0.8	<3.3E-04
Sz 77	CTTSs	−17.10	304	M0	TNIR	not SB	7	3850	2.41	5.30E+05	2.1	0.5	5.60E-02
RX J1552.3-3819	WTTSs	−0.70	174	K7	RJ			4050	0.71	2.70E+06	0.5	2.6	<8.2E-04
RX J1554.9-3827	WTTSs	−1.94	91	K7	RJ			4050	0.69	2.80E+06	0.6	2.1	<8.9E-04
PZ99 J155506.2-2521	WTTSs	−0.76	152	M1	RJ			3700	0.59	1.50E+06	0.4	5.0	<5.9E-04
RX J1555.4-3338	WTTSs	−1.20	95	K5	RJ	not SB	7	4350	0.97	4.20E+06	0.6	2.1	<9.4E-04
RX J1555.6-3709	WTTSs	−0.61	146	K6	RJ			4200	1.06	2.30E+06	0.4	2.2	<1.0E-03
Sz 81	CTTSs	−35.80	330	M5.5	TNIR			3200	0.65	7.90E+05	0.4	2.5	9.80E-02
RX J1556.1-3655	CTTSs	−82.60	416	M1	TNIR			3700	0.82	1.10E+06	1.5	1.9	9.70E-02
Sz 82	CTTSs	−39.00	–	M0	TNIR			3850	3.63	2.90E+05	1.4	2.2	1.00E-01
PZ99 J155702.3-1950	WTTSs	−0.81	159	K7	RJ			4050	0.79	2.30E+06	0.4	3.2	<2.8E-04
Sz 84	CTTSs	−43.70	422	M5.5	T24			3200	0.36	1.10E+06	0.8	2.3	7.70E-02
RX J1559.0-3646	WTTSs	−3.05	174	M1.5	RJ			3700	0.72	1.20E+06	0.1	2.2	<9.4E-04
Sz 129	CTTSs	−43.90	346	K8	TNIR			3950	2.12	6.20E+05	3.3	0.3	7.20E-02
RX J1559.8-3628	WTTSs	−0.45	103	K3	RJ			4700	3.86	1.90E+06	0.5	2.2	<2.4E-04
RX J1601.2-3320	WTTSs	−1.92	−137	G8	T24	not SB	7	5500	3.34	1.10E+07	0.3	3.2	7.20E-05
PZ99 J160151.4-2445	WTTSs	−0.07	141	K7	RJ			4050	0.76	2.40E+06	1.0	3.6	<3.4E-04
PZ99 J160158.2-2008	WTTSs	−1.50	−117	G5	RJ			5250	2.82	7.70E+06	1.2	2.2	<6.8E-05
RX J1602.0-3613	WTTSs	−0.85	–	K3	RJ			4700	1.81	4.60E+06	0.5	1.9	<3.4E-04
PZ99 J160253.9-2022	WTTSs	−2.77	180	K7	RJ			4050	1.03	1.60E+06	1.3	2.2	<2.2E-04

Table 1
(Continued)

ID	Type	EW(H_α) (Å)	FW.1H (km s^{-1})	SpT	SED Type	Bin. Notes	Bin. Ref.	$T_{\rm eff}$ (K)	$L_\star$ ($L_\odot$)	Age (yr)	A_v (mag)	$d_{\rm edge}$ (deg)	L_d/L_*
RX J1603.2-3239	WTTSs	−2.45	132	K7	T24			4050	1.04	1.60E+06	0.6	4.0	1.50E-03
RX J1603.8-4355	WTTSs	0.00	−212	G8V	RJ			5500	10.33	3.90E+06	0.4	0.3	<1.9E-04
RX J1603.8-3938	WTTSs	−0.03	153	K3	RJ			4700	3.17	2.40E+06	0.4	0.0	<9.7E-04
RX J1604.5-3207	WTTSs	−0.19	−74	K2	RJ			4900	2.45	4.70E+06	0.2	4.4	<2.3E-04
RX J1605.6-3837	WTTSs	−2.63	124	M1	RJ			3700	0.41	2.20E+06	0.3	0.5	<2.3E-03
PZ99 J160550.5-2533	WTTSs	−0.21	85	G7	RJ			5600	1.52	2.30E+04	0.7	2.6	<2.5E-04
RX J1607.2-3839	WTTSs	−2.39	181	K7	RJ			4050	1.28	1.20E+06	0.4	0.3	<7.7E-04
Sz 96	CTTSs	−6.10	369	M1.5	TNIR	not SB	11	3700	1.17	8.30E+05	1.9	−0.2	1.20E-01
RX J1608.3-3843	WTTSs	−1.04	131	K7	RJ	not SB	7	4050	1.52	9.80E+05	0.6	0.1	<5.3E-04
Sz 98	CTTSs	−29.10	382	K8	TNIR	not SB	7	3950	4.12	3.80E+05	4.4	−0.2	6.60E-02
RX J1608.5-3847	CTTSs	−6.17	438	M2	TIRAC			3550	1.38	6.40E+05	1.2	0.1	3.10E-02
RX J1608.6-3922	CTTSs	−14.20	656	K6	TNIR	not SB	7	4200	2.18	8.80E+05	3.0	0.0	3.90E-02
PZ99 J160843.4-2602	WTTSs	−0.32	−120	G7	RJ	not SB	7	5600	2.53	1.50E+07	0.7	1.8	<1.5E-04
RX J1609.7-3854	WTTSs	−0.39	137	K5	RJ			4350	3.42	7.50E+05	0.7	−0.1	<2.4E-04
Sz 117	CTTSs	−20.50	183	M2	TIRAC	<0.13	12	3550	0.74	1.00E+06	2.3	−0.2	5.30E-02
RX J1610.1-4016	WTTSs	−0.27	192	K2	RJ			4900	2.42	4.80E+06	0.5	0.3	<3.8E-04
PZ99 J161019.1-2502	WTTSs	−0.75	132	M1	RJ			3700	0.67	1.30E+06	0.3	1.8	<5.3E-04
WA Oph1	WTTSs	−1.70	137	K2	RJ	145 days	7	4900	2.74	4.10E+06	2.6	0.1	<7.0E-04
RX J1612.0-1906A	WTTSs	−0.50	−156	K3	RJ			4700	1.55	5.60E+06	1.4	0.3	<3.9E-04
RX J1612.1-1915	WTTSs	−1.80	139	K5	RJ			4350	0.75	6.10E+06	2.8	0.4	<6.6E-04
RX J1612.3-1909	WTTSs	−18.00	246	M2.5	RJ	SB	4	3550	0.22	3.30E+06	1.3	0.4	<2.6E-03
RX J1612.6-1924	WTTSs	−2.40	131	K8	T24	SB	4	3950	0.61	2.70E+06	1.7	0.4	6.80E-04
RX J1613.1-1904A	WTTSs	−2.70	117	M4	RJ	0.5	4	3350	0.18	3.00E+06	0.5	0.2	<2.5E-03
RX J1613.7-1926	WTTSs	−2.90	153	M1	RJ	0.7	4	3700	0.46	1.90E+06	1.5	0.3	<9.2E-04
RX J1613.8-1835	WTTSs	−7.60	–	M2e	RJ	<0.13	4	3550	0.18	4.40E+06	2.1	0.2	<3.2E-03
RX J1613.9-1848	WTTSs	−1.50	128	M2	RJ	<0.13	4	3550	0.16	5.00E+06	0.7	0.0	<4.3E-03
RX J1614.2-1938	WTTSs	−0.60	−91	K2	RJ			4900	0.02	2.90E+08	0.7	0.4	<3.0E-02
RX J1614.4-1857A	WTTSs	0.08	153	M2	T24	<0.13	4	3550	0.01	4.50E+04	4.2	−0.2	3.90E-03
RX J1615.1-1851	WTTSs	−2.60	121	K7-M0	RJ	<0.13	4	3900	0.63	2.00E+06	9.2	0.0	<7.0E-04
RX J1615.3-3255	CTTSs	−18.90	397	K5	TIRAC			4350	2.11	1.40E+06	1.1	2.5	7.00E-02
RX J1621.2-2342A	WTTSs	−0.80	142	K7	RJ			4050	0.54	4.20E+06	2.2	−0.1	<3.6E-03
RX J1621.2-2342B	WTTSs	−0.80	–	K7	RJ			4050	0.92	1.90E+06	7.8	−0.1	<3.1E-03
RX J1621.4-2312	WTTSs	−1.60	181	K7	RJ			4050	0.72	2.70E+06	2.7	0.0	<1.1E-03
RX J1622.6-2345	WTTSs	−3.60	128	M2.5	T24	<0.13	4	3550	0.23	3.30E+06	2.7	−0.4	1.80E-03
RX J1622.7-2325A	WTTSs	−1.70	124	M1	RJ	SB	4	3700	1.15	8.40E+05	4.4	−0.4	<5.0E-03
RX J1622.7-2325B	WTTSs	−4.10	–	M3	RJ	SB	4	3450	0.27	2.30E+06	3.9	−0.4	<1.6E-02
RX J1622.8-2333	WTTSs	−1.70	91	K8	RJ	SB	4	3950	0.47	4.00E+06	4.8	−0.4	<6.3E-03
RX J1623.5-3958	WTTSs	−2.53	−313	G0	RJ			6000	2.81	1.90E+07	0.7	−0.3	<3.8E-04
RX J1623.8-2341	WTTSs	−0.40	197	K5	RJ			4350	1.10	3.40E+06	4.2	−0.7	<3.2E-03
RX J1624.0-2456	WTTSs	−0.92	153	K0	RJ			5250	2.03	1.10E+07	3.4	−0.5	2.60E-05
RX J1624.8-2359	WTTSs	−0.06	0	K3	RJ			4700	2.95	2.60E+06	5.4	−0.6	<1.1E-03
RX J1625.2-2455	WTTSs	−2.90	206	M0	RJ	<0.13		3850	1.03	1.00E+06	3.0	−0.4	<1.1E-03
EM*SR8	WTTSs	−1.30	129	K2	RJ	<0.13	5	4900	1.20	1.10E+07	3.2	−0.6	<3.0E-03
DOAR21	WTTSs	−0.70	−197	B2V	TIRAC	<0.005	2;5	22000	1477.07	1.00E+05	12.4	−0.7	3.50E-04
ROXR123	CTTSs	−16.10	489	K7	TNIR	<0.13	5	4050	2.02	7.20E+05	4.7	−0.6	4.50E-02
ROX16	CTTSs	−10.00	–	B5	TNIR	0.577	5	15400	201.20	1.00E+05	14.0	−0.6	2.20E-04
ROXR135S	CTTSs	−73.00	–	K7	TNIR	0.197	2;5	4050	5.80	3.30E+05	12.2	−0.6	1.20E-01
ROX21	CTTSs	−3.00	–	Me	RJ	0.3	2;5	3200	1.03	1.60E+04	7.1	−0.5	<3.4E-03
ROXR151B	WTTSs	−3.70	–	M0	TNIR	<0.13	4	3350	1.23	1.20E+05	8.7	−0.4	1.50E-01
EM*SR9	CTTSs	−6.40	394	K3.5e	TNIR	0.638	5	4700	4.31	1.70E+06	3.3	−0.4	4.60E-02
NTTS162649-2145	WTTSs	−0.20	234	K0	RJ			5250	2.83	7.60E+06	2.0	0.6	<1.9E-04
ROX39	CTTSs	−3.60	–	K5	RJ	<0.13	5	4350	1.51	2.10E+06	2.2	−0.1	<3.7E-04
ROXS42C	WTTSs	−1.60	183	M	TIRAC	0.277	5	3200	3.80	1.30E+04	8.3	−0.2	2.10E-02
ROXS43A	WTTSs	−1.80	–	G8+...	TIRAC	89 days	7	5500	9.84	4.10E+06	3.7	−0.2	4.50E-02
ROXS47A	WTTSs	−9.20	–	K8	TIRAC	0.046	13	3950	1.54	8.30E+05	3.2	−0.4	1.10E-02
WA Oph6	CTTSs	−17.05	442	K7	TNIR			4050	6.06	3.10E+05	6.5	−0.3	3.90E-02

Notes. FW.1H: notes of the full width at 10% of H alpha line. (Keller 2004; 0* indicates non detections). Negative velocities indicate absorption. Bin. notes: the separation of binary component is arcseconds or their period in days. Limits on non detection are also given; e.g., <0.13 indicates a companion is only possible for $\rho < 0\farcs13$. Binary references: 1. Leinert et al. 1993, 2. Simon et al. 1995, 3. Lafrenière et al. 2008, 4. Prato 2007, 5. Ratzka et al. 2005, 6. Köhler 2001, 7. Guenther et al. 2007, 8. Kohler & Leinert 1998, 9. Sartoretti et al. 1998, 10. Steffen et al. 2001, 11. Melo 2003, 12. Ghez et al. 1997, 13. Barsony et al. 2003. $d_{\rm edge}$: distance from cloud edge in degrees. Negative numbers indicate that objects are within cloud boundary as defined in the text.

Table 2
2MASS and *Spitzer* Photometry

ID	R.A. (hh mm ss.s)	Decl. (dd mm ss.s)	F_J (mJy)	F_H (mJy)	F_K (mJy)	$F_{3.6}$ (mJy)	$F_{4.5}$ (mJy)	$F_{5.8}$ (mJy)	F_8 (mJy)	F_{24} (mJy)	F_{70} (mJy)
NTTS032641+2420	03 29 38.4	+24 30 37.8	119	117	88	38	24.2	16.0	9.9	1.1	<18
NTTS040047+2603	04 03 50.9	+26 10 53.0	113	129	103	52	32	23.8	14.2	1.6	<11
RX J0405.3+2009	04 05 19.6	+20 09 25.6	534	542	386	144	98	69	43	5.1	<10
NTTS040234+2143	04 05 30.9	+21 51 10.7	67	78	63	30.3	20.5	14.8	8.5	1.0	<20
RX J0409.2+1716	04 09 17.0	+17 16 08.2	166	204	160	74	47	33	19.2	1.8	<15
RX J0409.8+2446	04 09 51.1	+24 46 20.9	146	169	133	57	40	27.1	17.0	2.6	<30
RX J0412.8+1937	04 12 50.6	+19 36 57.9	160	172	134	54	35	22.7	13.1	2.0	<24
LkCa 1	04 13 14.2	+28 19 10.7	222	291	237	97	68	50	31.1	2.7	<10
LkCa 3	04 14 48.0	+27 52 34.6	720	913	716	324	208	150	90	9.5	<9
LkCa 5	04 17 39.0	+28 33 00.4	163	197	159	75	51	35	20.6	2.5	<9
NTTS041559+1716	04 18 51.7	+17 23 16.6	156	175	131	56	36	25.0	15.7	1.6	<10
LkCa 7	04 19 41.3	+27 49 48.4	357	455	332	125	108	76	45	5.6	<19
RX J0420.3+3123	04 20 24.1	+31 23 23.7	105	115	86	40	25.1	16.2	10.7	1.0	<19
HD 283572	04 21 58.9	+28 18 06.3	1730	1610	1190	485	326	228	133	14.7	<10
LkCa 21	04 22 03.2	+28 25 38.9	261	348	278	125	91	65	39	4.9	<29
RX J0424.8+2643	04 24 49.0	+26 43 10.4	574	650	514	219	157	104	61	6.7	<34
NTTS042417+1744	04 27 10.6	+17 50 42.6	489	450	320	109	74	57	34	3.7	<9
DH Tau	04 29 41.6	+26 32 58.2	198	302	357	269	207	172	133	319	384 ± 67
DI Tau	04 29 42.5	+26 32 49.2	297	372	293	133	77	64	38	4.2	<346
UX Tau	04 30 04.0	+18 13 49.5	567	670	636	544	391	406	262	1210	2643 ± 407
FX Tau	04 30 29.6	+24 26 44.9	280	448	451	373	299	266	330	414	317 ± 57
ZZ Tau	04 30 51.4	+24 42 22.3	254	341	280	122	118	109	115	118	<244
V927 Tau	04 31 23.8	+24 10 52.8	205	243	207	95	70	53	31.0	3.6	<8
NTTS042835+1700	04 31 27.2	+17 06 24.7	124	134	106	47	32	21.2	12.6	1.3	<10
V710 Tau	04 31 57.8	+18 21 38.2	310	233	230	202	141	169	134	236	343 ± 61
NTTS042916+1751	04 32 09.3	+17 57 22.7	210	244	192	80	54	40	23.5	2.4	<10
V928 Tau	04 32 18.8	+24 22 27.0	244	434	382	152	123	88	59	6.7	<19
NTTS042950+1757	04 32 43.7	+18 02 56.2	138	168	126	58	37	26.5	16.2	2.0	<10
RX J0432.8+1735	04 32 53.2	+17 35 33.7	159	208	164	80	45	35	22.4	16.9	<28
GH Tau	04 33 06.2	+24 09 33.8	362	521	509	389	352	330	285	345	433 ± 75
V807 Tau	04 33 06.6	+24 09 54.9	879	1170	1100	662	568	539	449	420	621 ± 103
V830 Tau	04 33 10.0	+24 33 42.9	297	367	285	94	73	53	32	3.7	<14
GK Tau	04 33 34.6	+24 21 05.8	381	585	687	702	630	551	751	1510	1126 ± 180
WA Tau1	04 34 39.3	+25 01 01.1	682	688	506	159	124	91	48	6.3	<8
NTTS043230+1746	04 35 24.5	+17 51 42.9	155	191	156	75	51	35	21.1	2.2	···
RX J0435.9+2352	04 35 56.8	+23 52 05.0	224	269	222	90	70	49	30.6	3.5	<19
LkCa 14	04 36 19.1	+25 42 58.9	294	335	247	103	67	42	28.7	3.0	<13
RX J0437.4+1851	04 37 26.9	+18 51 26.7	271	386	228	104	62	48	29.1	3.7	<22
RX J0438.2+2023	04 38 13.0	+20 22 47.2	149	157	120	54	35	22.3	14.4	1.3	<14
HV Tau	04 38 35.3	+26 10 38.5	325	497	459	190	147	117	69	18.0	<500
RX J0438.6+1546	04 38 39.1	+15 46 13.6	439	465	338	144	78	60	37	4.9	<16
RX J0439.4+3332A	04 39 25.9	+33 32 19.4	18.1	24.7	19.1	9.1	5.8	3.9	2.5	0.1	<19
IW Tau	04 41 04.7	+24 51 06.1	320	416	327	132	100	73	44	4.9	<10
ITG33	04 41 08.3	+25 56 07.4	5.1	14.2	24.5	32	38	40	52	94	113 ± 26
HBC422	04 42 05.5	+25 22 56.2	194	351	341	136	128	93	57	7.7	264 ± 50
HBC423	04 42 07.8	+25 23 11.8	190	371	444	410	470	432	488	476	1180 ± 190
RX J0445.8+1556	04 45 51.3	+15 55 49.7	1150	1060	775	329	198	145	88	8.1	<134
RX J0452.5+1730	04 52 30.7	+17 30 25.8	164	176	133	55	36	25.0	15.8	1.4	<10
RX J0452.8+1621	04 52 50.1	+16 22 09.1	365	413	326	121	97	64	40	4.4	<10
LkCa 19	04 55 37.0	+30 17 55.0	451	482	367	112	98	69	42	10.5	<21
NTTS045251+3016	04 56 02.0	+30 21 03.5	416	483	374	183	-	-	-	5.1	<38
RX J0457.2+1524	04 57 17.7	+15 25 09.4	708	705	529	250	135	100	60	7.6	<19
RX J0457.5+2014	04 57 30.6	+20 14 29.6	309	302	223	95	61	43	26.2	2.5	<15
RX J0458.7+2046	04 58 39.7	+20 46 44.0	232	267	201	82	56	38	22.2	3.0	<26
RX J0459.7+1430	04 59 46.2	+14 30 55.4	219	236	176	77	47	34	20.4	1.8	<10
V836 Tau	05 03 06.6	+25 23 19.9	173	240	243	134	105	110	126	193	220 ± 42
RX J0842.4-8345	08 42 22.7	−83 45 24.5	264	312	243	90	72	48	29.6	3.4	<28
RX J0848.0-7854	08 47 56.8	−78 54 53.3	297	344	288	74	74	68	40	4.7	<5
RX J0902.9-7759	09 02 51.3	−77 59 34.8	145	169	136	64	41	31.3	17.6	2.6	<19
RX J0915.5-7609	09 15 29.1	−76 08 47.1	297	346	268	99	78	56	34	3.5	<43
RX J0935.0-7804	09 34 56.0	−78 04 19.4	193	228	185	91	63	42	24.3	2.6	<6
RX J0942.7-7726	09 42 49.6	−77 26 40.8	114	137	109	49	33	21.8	13.4	1.5	<17
RX J1001.1-7913	10 01 08.7	−79 13 07.6	150	181	137	57	41	29.7	16.8	2.2	<6
RX J1005.3-7749	10 05 20.0	−77 48 42.3	191	239	185	81	58	38	23.7	2.8	<6
CS Cha	11 02 24.9	−77 33 35.6	363	426	350	126	99	72	48	617	2543 ± 393

Table 2
(Continued)

ID	R.A. (hh mm ss.s)	Decl. (dd mm ss.s)	F_J (mJy)	F_H (mJy)	F_K (mJy)	$F_{3.6}$ (mJy)	$F_{4.5}$ (mJy)	$F_{5.8}$ (mJy)	F_8 (mJy)	F_{24} (mJy)	F_{70} (mJy)
RX J1108.8-7519	11 08 53.3	−75 19 37.5	203	250	201	104	64	44	27.9	3.1	<20
Sz 30	11 09 11.8	−77 29 12.5	170	225	174	92	57	41	26.3	3.2	<20
Sz 41	11 12 24.3	−76 37 06.6	311	399	421	243	239	225	317	278	89 ± 21
RX J1117.0-8028	11 16 57.1	−80 27 52.1	186	202	174	97	66	45	26.8	3.4	<5
RX J1123.2-7924	11 23 10.6	−79 24 43.3	29.2	25.8	17.0	7.7	5.5	3.3	1.9	0.1	<16
RX J1129.2-7546	11 29 12.6	−75 46 26.4	189	229	187	88	58	37	22.6	2.5	<28
RX J1149.8-7850	11 49 31.8	−78 51 00.9	265	333	269	165	173	190	366	1240	1227 ± 194
RX J1150.4-7704	11 50 28.3	−77 04 38.3	207	227	172	81	50	34	20.5	2.2	<12
T Cha	11 57 13.5	−79 21 31.5	417	735	1100	1410	1290	1110	708	1740	–
RX J1158.5-7754	11 58 28.3	−77 54 29.1	822	973	728	325	207	143	87	9.3	<16
RX J1158.5-7913	11 58 34.3	−79 13 17.6	202	267	231	101	73	53	32	4.9	<30
RX J1159.7-7601	11 59 42.3	−76 01 26.2	352	419	318	125	99	62	40	4.7	–
RX J1202.1-7853	12 02 03.7	−78 53 01.3	328	425	317	160	106	75	46	5.2	<12
RX J1204.6-7731	12 04 36.1	−77 31 34.7	198	229	187	80	64	44	26.5	3.4	<18
RX J1216.8-7753	12 16 45.9	−77 53 33.4	146	168	135	60	42	28.1	17.1	2.0	<7
RX J1219.7-7403	12 19 43.7	−74 03 57.4	201	246	191	94	58	42	25.2	2.8	<7
RX J1220.4-7407	12 20 21.8	−74 07 39.6	315	369	300	141	95	66	40	4.7	<9
RX J1239.4-7502	12 39 21.3	−75 02 39.3	674	675	517	215	138	95	57	6.2	<8
RX J1301.0-7654	13 00 56.3	−76 54 02.2	389	497	385	188	135	91	54	6.2	<102
RX J1507.6-4603	15 07 37.8	−46 03 15.8	188	212	153	72	46	31.3	18.5	1.9	<21
RX J1508.6-4423	15 08 37.7	−44 23 17.2	288	276	200	85	52	38	23.2	2.4	<7
RX J1511.6-3550	15 11 37.0	−35 50 42.0	145	159	123	57	38	25.3	14.8	1.6	<8
RX J1515.8-3331	15 15 45.4	−33 31 59.9	407	423	295	116	80	57	32	4.4	<27
RX J1515.9-4418	15 15 52.8	−44 18 17.5	135	152	110	48	29.8	19.8	13.0	1.4	<8
RX J1516.6-4406	15 16 36.6	−44 07 20.6	175	192	140	54	38	26.3	15.7	1.6	<22
RX J1518.9-4050	15 18 52.8	−40 50 52.9	350	352	254	99	69	49	29.6	3.3	<26
RX J1519.3-4056	15 19 16.0	−40 56 07.7	241	252	196	88	57	40	23.7	2.4	<11
RX J1522.2-3959	15 22 11.6	−39 59 51.1	174	196	153	68	44	30.0	18.2	2.0	<7
RX J1523.4-4055	15 23 25.6	−40 55 46.9	166	180	132	60	37	25.8	15.1	1.6	<10
RX J1523.5-3821	15 23 30.4	−38 21 28.9	110	135	106	48	34	23.9	14.1	1.8	<10
RX J1524.0-3209	15 24 03.1	−32 09 51.0	252	304	232	105	69	50	29.5	3.2	<17
RX J1524.5-3652	15 24 32.4	−36 52 02.9	241	246	179	79	49	33	20.0	2.2	<7
RX J1525.5-3613	15 25 33.2	−36 13 46.9	238	256	194	78	57	39	24.6	2.7	<15
RX J1525.6-3537	15 25 36.7	−35 37 32.0	195	227	173	70	50	34	20.7	2.2	<10
RX J1526.0-4501	15 25 59.7	−45 01 16.0	266	261	183	75	48	33	20.4	2.0	<10
RX J1538.0-3807	15 38 02.7	−38 07 23.2	144	152	118	49	34	23.8	14.8	1.6	<14
RX J1538.6-3916	15 38 38.3	−39 16 55.5	232	255	192	84	50	35	21.2	2.2	<10
RX J1538.7-4411	15 38 43.1	−44 11 47.6	479	471	347	140	91	62	36	4.4	<22
Sz 65	15 39 27.8	−34 46 17.4	336	441	428	255	225	231	284	502	533 ± 90
RX J1540.7-3756	15 40 41.2	−37 56 18.7	170	191	141	62	39	26.4	16.2	1.6	<10
RX J1543.1-3920	15 43 06.3	−39 20 19.6	184	211	153	63	46	30.8	18.0	1.5	<24
RX J1546.7-3618	15 46 41.2	−36 18 47.5	255	270	205	95	59	41	25.3	2.4	<11
RX J1547.7-4018	15 47 41.8	−40 18 27.0	305	306	229	92	62	44	25.1	2.6	<23
PZ99 J154920.9-260005	15 49 21.0	−26 00 06.5	555	575	456	198	119	84	53	5.4	<45
Sz 76	15 49 30.7	−35 49 51.7	66	79	65	35	26.2	23.5	34	63	204 ± 39
RX J1550.0-3629	15 49 59.2	−36 29 57.6	239	252	186	80	52	37	21.7	2.5	<12
Sz 77	15 51 46.9	−35 56 44.3	266	375	328	218	181	170	199	333	175 ± 35
RX J1552.3-3819	15 52 19.5	−38 19 31.6	115	137	103	46	30.6	20.4	12.7	1.2	<9
RX J1554.9-3827	15 54 52.9	−38 27 56.8	109	130	99	46	30.7	21.4	13.2	1.4	<9
PZ99 J155506.2-252109	15 55 06.3	−25 21 10.4	274	366	263	106	78	56	33	3.5	<37
RX J1555.4-3338	15 55 26.2	−33 38 23.4	138	156	121	54	32	23.6	14.5	1.9	<27
RX J1555.6-3709	15 55 33.8	−37 09 41.3	165	190	144	63	40	27.4	16.2	1.5	<22
Sz 81	15 55 50.3	−38 01 33.6	135	157	143	103	96	74	80	95	183 ± 36
RX J1556.1-3655	15 56 02.1	−36 55 28.4	111	149	127	88	72	59	68	205	242 ± 45
Sz 82	15 56 09.2	−37 56 06.5	489	595	535	324	220	313	370	765	1458 ± 229
PZ99 J155702.3-195042	15 57 02.4	−19 50 42.2	340	412	299	145	96	63	37	3.9	<11
Sz 84	15 58 02.5	−37 36 02.9	68	85	76	43	29.5	20.5	12.5	24.3	377 ± 66
RX J1559.0-3646	15 58 59.8	−36 46 20.9	140	168	129	68	42	30.9	18.6	1.6	<10
Sz 129	15 59 16.5	−41 57 10.5	170	238	240	178	157	136	184	326	483 ± 82
RX J1559.8-3628	15 59 49.5	−36 28 28.0	494	563	410	175	111	82	48	6.0	<35
RX J1601.2-3320	16 01 09.0	−33 20 14.3	391	389	259	109	67	48	28.6	4.9	<9
PZ99 J160151.4-244524	16 01 51.5	−24 45 25.2	275	352	269	125	75	56	33	3.6	<11
PZ99 J160158.2-200811	16 01 58.2	−20 08 12.2	729	771	569	193	142	123	67	7.4	<12
RX J1602.0-3613	16 01 59.2	−36 12 55.8	231	264	192	88	58	41	24.4	2.5	<12
PZ99 J160253.9-202248	16 02 54.0	−20 22 48.2	345	421	353	156	113	88	49	5.7	<9

Table 2
(Continued)

ID	R.A. (hh mm ss.s)	Decl. (dd mm ss.s)	F_J (mJy)	F_H (mJy)	F_K (mJy)	$F_{3.6}$ (mJy)	$F_{4.5}$ (mJy)	$F_{5.8}$ (mJy)	F_8 (mJy)	F_{24} (mJy)	F_{70} (mJy)
RX J1603.2-3239	16 03 11.8	−32 39 20.4	163	196	149	67	44	35	20.9	9.2	<27
RX J1603.8-4355	16 03 45.4	−43 55 49.3	1080	1110	791	337	213	150	95	10.5	<40
RX J1603.8-3938	16 03 52.5	−39 39 01.5	423	466	342	125	94	65	39	4.2	<49
RX J1604.5-3207	16 04 30.6	−32 07 28.9	343	342	250	125	73	52	31.4	3.3	<21
RX J1605.6-3837	16 05 33.3	−38 37 45.4	77	93	73	36	22.8	16.0	9.9	1.3	<12
PZ99 J160550.5-253313	16 05 50.7	−25 33 13.8	362	376	275	109	74	53	31.2	3.5	<12
RX J1607.2-3839	16 07 13.7	−38 39 24.0	212	267	188	87	59	42	25.7	3.6	<16
Sz 96	16 08 12.6	−39 08 33.5	142	187	174	168	113	138	173	231	154 ± 33
RX J1608.3-3843	16 08 18.3	−38 44 05.5	238	277	218	102	66	46	26.9	3.3	<13
Sz 98	16 08 22.5	−39 04 46.3	246	354	415	373	477	429	693	28.5	496 ± 85
RX J1608.5-3847	16 08 31.6	−38 47 29.5	215	275	237	132	94	73	55	162	48 ± 16
RX J1608.6-3922	16 08 36.2	−39 23 02.6	177	247	229	153	138	132	132	113	462 ± 80
PZ99 J160843.4-260216	16 08 43.4	−26 02 17.0	606	617	458	197	112	90	52	5.9	<19
RX J1609.7-3854	16 09 39.5	−38 55 07.4	471	534	422	189	112	81	50	7.2	<14
Sz 117	16 09 44.3	−39 13 30.3	86	118	113	65	62	57	55	92	127 ± 28
RX J1610.1-4016	16 10 04.8	−40 16 12.4	293	310	238	97	65	48	29.0	2.8	<20
PZ99 J161019.1-250230	16 10 19.2	−25 02 30.4	317	394	301	124	86	61	36	3.6	<28
WA Oph1	16 11 08.9	−19 04 47.1	499	656	558	291	163	121	74	8.4	<19
RX J1612.0-1906A	16 11 59.3	−19 06 53.5	407	482	386	121	105	74	43	5.3	<35
RX J1612.1-1915	16 12 05.3	−19 15 20.0	153	239	190	87	52	40	23.3	2.1	<18
RX J1612.3-1909	16 12 20.9	−19 09 04.3	84	115	96	48	33	23.7	14.0	1.6	<17
RX J1612.6-1924	16 12 41.2	−19 24 18.5	187	239	207	93	69	50	28.8	8.9	<35
RX J1613.1-1904A	16 13 10.2	−19 04 13.3	89	102	92	50	35	23.1	14.2	1.9	<18
RX J1613.7-1926	16 13 43.9	−19 26 48.7	161	209	183	86	58	43	25.0	2.9	<21
RX J1613.8-1835	16 13 47.5	−18 35 00.6	57	80	72	38	26.6	17.7	11.0	1.3	<12
RX J1613.9-1848	16 13 58.2	−18 48 29.3	73	97	74	37	25.3	18.7	10.1	1.1	<39
RX J1614.2-1938	16 14 14.0	−19 38 28.3	6.5	7.3	5.5	2.5	1.6	1.1	0.7	0.0	<14
RX J1614.4-1857A	16 14 30.0	−18 57 41.9	1.0	1.7	1.7	0.9	0.7	0.6	0.3	0.3	<37
RX J1615.1-1851	16 15 08.6	−18 51 01.2	76	118	102	54	35	24.6	15.4	0.0	<14
RX J1615.3-3255	16 15 20.2	−32 55 05.3	268	316	252	98	85	65	73	322	1049 ± 167
RX J1621.2-2342A	16 21 14.5	−23 42 20.0	145	200	169	92	56	39	23.4	2.1	<78
RX J1621.2-2342B	16 21 15.4	−23 42 26.5	56	145	159	97	59	45	27.3	3.4	<115
RX J1621.4-2312	16 21 28.4	−23 12 11.0	169	250	213	110	71	51	30.7	2.8	<25
RX J1622.6-2345	16 22 37.6	−23 45 50.8	60	97	85	44	32	22.1	13.9	6.5	<48
RX J1622.7-2325A	16 22 46.8	−23 25 33.0	190	354	339	208	144	92	55	6.7	<208
RX J1622.7-2325B	16 22 47.2	−23 25 44.9	54	98	93	54	36	25.8	16.0	1.6	<261
RX J1622.8-2333	16 22 53.3	−23 33 10.3	65	115	117	61	43	29.7	17.9	1.8	<54
RX J1623.5-3958	16 23 29.6	−39 58 01.0	261	236	170	70	49	33	19.6	2.2	<14
RX J1623.8-2341	16 23 49.4	−23 41 27.1	158	254	242	129	87	62	38	4.8	<424
RX J1624.0-2456	16 24 06.3	−24 56 47.0	266	373	325	152	109	74	47	7.7	<33
RX J1624.8-2359	16 24 48.4	−23 59 16.0	269	502	480	266	171	120	72	7.4	<118
RX J1625.2-2455	16 25 14.7	−24 56 07.0	233	379	328	171	112	81	49	5.5	<47
EM*SR8	16 25 26.9	−24 43 09.0	186	263	229	107	69	49	30.0	2.5	<157
DOAR21	16 26 03.0	−24 23 36.0	926	1840	2150	1260	878	743	689	1810	<1786
ROXR123	16 26 23.7	−24 43 14.0	279	448	484	367	292	299	258	399	956 ± 173
ROX16	16 26 46.4	−24 11 59.9	214	487	676	603	355	495	386	278	<311
ROXR135S	16 26 58.4	−24 45 31.8	114	360	637	1390	1440	1740	1950	2230	5416 ± 829
ROX21	16 27 19.5	−24 41 40.2	271	361	289	140	95	68	40	5.2	<2063
ROXR151A	16 27 39.4	−24 39 15.3	80	211	274	282	284	333	427	1140	1458 ± 231
EM*SR9	16 27 40.3	−24 22 04.0	671	878	873	784	575	465	484	1040	<860
NTTS162649-2145	16 29 48.7	−21 52 12.0	539	644	527	238	148	105	64	7.3	<23
ROX39	16 30 35.6	−24 34 18.7	367	500	411	197	138	98	58	6.3	<52
ROXS42C	16 31 15.7	−24 34 02.0	724	1010	938	575	428	371	397	862	239 ± 53
ROXS43A	16 31 20.1	−24 30 04.9	1100	1390	1360	4.6	800	895	1970	2180	938 ± 152
ROXS47A	16 32 11.8	−24 40 21.5	320	468	449	265	212	152	122	105	171 ± 41
WA Oph6	16 48 45.6	−14 16 35.9	519	957	1200	1090	814	966	1010	1270	1298 ± 205

Notes. The absolute calibration uncertainties in the IRAC bands and the MIPS-24 μm band are 5% and 10%, respectively. These calibration uncertainties are typically more than twice the random errors and thus dominate the total photometric uncertainty.

from the nearby star, GSC 01267-00433. For RX J0842.4-8345, the 70 μm flux clearly originates from a separate nearby source which appears clearly resolved at 8 μm. In the case of RX J1129.2-7546, there is confusion from a known nearby source 8″ to the East (2M J11291470-7546256; Luhman et al. 2008), which appears at 3.6 μm and begins to dominate at

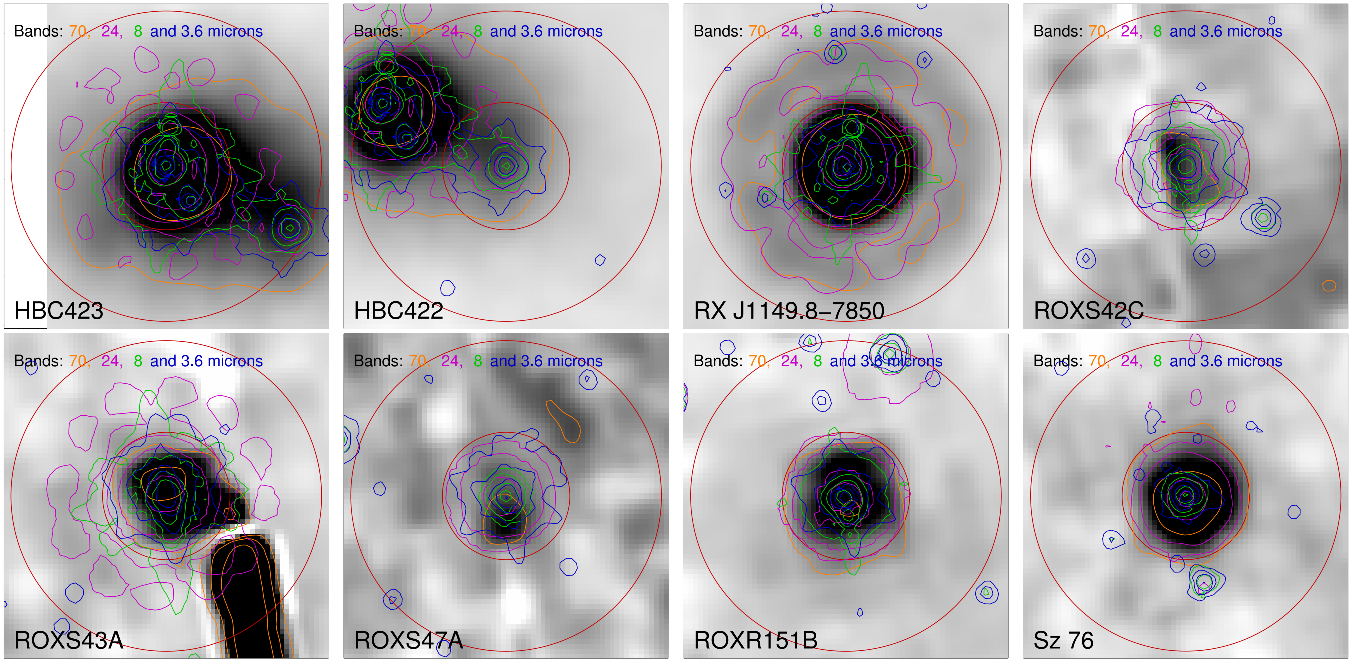

Figure 1. 70 μm images of the detected WTTSs targets. North is up and East is left. Contour map overlays from the IRAC1, IRAC4, MIPS-24 μm and MIPS-70 μm bands are shown in blue, green, pink, and orange, respectively. The contour levels shown are at 3, 15, 75, and 375 times the background root mean square. The red circles represent the 16″ (radius) object aperture and the 39″ outer sky aperture used for photometry. The 18″ inner sky aperture is not shown.

(A color version of this figure is available in the online journal.)

24 μm. False detection of RX J1301.0-7654 was also caused by the nearby YSO, 2MASS J13005323-7654151. Near WA Oph1, a faint resolved 24 μm source appears 8″ to the North, and although its location does not match well with the 70 μm emission, it is a better match to the emission than our target. A similar situation arises in the case of RX J1612.0-1906A. For RX J1621.2-2342a, RX J1623.8-2341, ROX16 and SR9, it is clear that there is too much nearby nebulosity to be confident that 70 μm detections are associated with circumstellar disks. In some cases, the nebulosity is already seen at 8 and 24 μm and gets stronger at longer wavelengths. Photometry at 70 μm was not obtained for NTTS 043230+1746 and RX J1159.7-7601, as the c2d *Spitzer* observations had the wrong pointings for these objects.

3. RESULTS

3.1. Estimating Infrared Excess

Targets with redder colors than main-sequence stars imply emission due to warm dust. The warmer the dust, the shorter the wavelength at which the excess is observed. As in the previous c2d papers on WTTSs (Padgett et al. 2006), we look for color excess using the 2MASS and *Spitzer* bands. First, we look at $K-[24]$ colors, since the MIPS-24 μm band is our most sensitive band to typical circumstellar dust emission.

The stellar K-band magnitudes have to be corrected for extinction before we calculate $K-[24]$ colors since many of our targets are embedded in their parent star-forming clouds. We use $A_V = 5.88E(J-K)$ to estimate the extinction for our sources, where $E(J-K)$ is the excess in $J-K$ color with respect to the expected stellar photosphere. The main-sequence $J-K$ colors are from Kenyon & Hartmann (1995). Extinction corrections were made according to Indebetouw et al. (2005), who based their empirical law on IRAC data from the GLIMPSE (Galactic Legacy Infrared Mid-Plane Survey Extraordinaire) project. The law is recommended for 2MASS and IRAC bands and relates A_λ to A_K as shown in Table 3. The derived extinctions A_V are displayed in Table 1. Extinction in the K band is below 0.2 mag for most our objects but some have very high extinctions. Thus, corrections to the $K-[24]$ colors were applied, even though adding extinction correction introduces noise into the $K-[24]$ color estimates, thus reducing our sensitivity to photospheric excess. There are 49 sources with $A_V > 2$ in our sample. We note that other than foreground cloud material, extinction could also result from occultation by an optically thick circumstellar disk.

Table 3
Relative Extinction in Optical, 2MASS, and *Spitzer* Bands

Band	V	J	H	K	IRAC1	IRAC2	IRAC3	IRAC4
A_λ/A_k	8.8	2.5	1.54	1.0	0.57	0.44	0.41	0.37

While the photospheric $K-[24]$ color for A to G dwarfs is almost zero, it can be up to 1 mag for an M dwarf, thus it is important to subtract the intrinsic photospheric colors before determining excess. The estimated $K-[24]$ colors for the photosphere were taken from Gautier et al. (2007). The photospheric colors $K-L$, $K-M$ and $K-N$ were also available from Kenyon & Hartmann (1995), and these were used for color corrections in the IRAC bands. Now, even though the exposure times were enough to robustly detect the photosphere at 24 μm, 6 of our 154 WTTSs are close to the confusion limit. To estimate the excess in the 24 μm band, we select the objects brighter than 0.5 mJy at 24 μm, a flux level at which we are assured negligible spurious detections and better than 95% completeness (Papovich et al. 2004). We end up with 148 WTTSs and 33 CTTSs with reliable $K-[24]$ colors. The rejected objects were RX J0439.4+3332a, RX J1123.2-7924, RX J1614.2-1938, RX J1614.4-1857a, and RX J1615.1-1851.

After subtracting the photospheric colors, we get a robust median (rejecting outliers) of 0.03 mag for the $K-[24]$ colors,

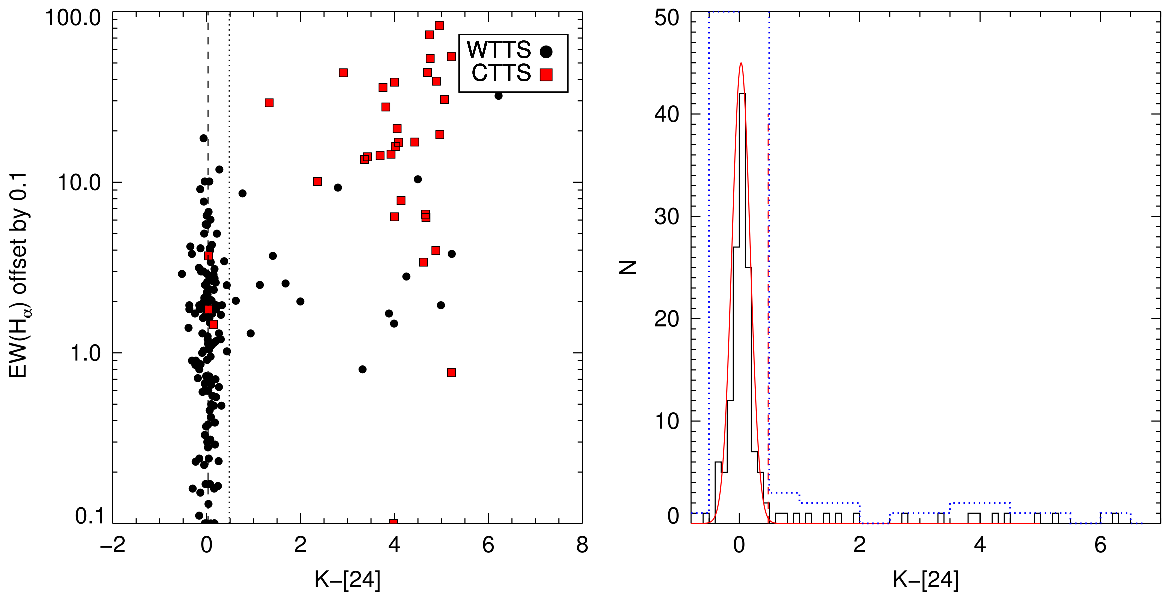

Figure 2. Left: EW(Hα) vs. the excess $K-[24]$ color for our sample of 181 stars. 148 WTTSs are shown as circles. 33 CTTSs are shown are squares. The EW($H\alpha$) come from low-resolution spectra, but the CTTS classification is adjusted using FW.1H($H\alpha$) estimated from high-resolution spectra. The dashed line shows the median color for the objects without excess. The dotted line is the 3σ marker for excess identification. A negligible offset has been added to the EW(Hα) values to allow easier plotting. Right: a histogram of $K-[24]$ excess for just the WTTSs. The solid red curve is a Gaussian with mean at $K-[24] = 0.02$ mag, and 1σ dispersion of 0.15 mag. The blue dotted line histogram is just a coarser binning of the same distribution. (Caution: it extends beyond the plot boundary at the peak of the distribution).

(A color version of this figure is available in the online journal.)

and a robust standard deviation of 0.15 mag. Throughout this paper, we identify the sources with excess color by looking at the color distribution itself. This method has been demonstrated in earlier *Spitzer* papers (Su et al. 2006; Padgett et al. 2006; Cieza et al. 2007). Most of our sources exhibit bare photospheres and should have zero excess colors. This group manifests itself as a Gaussian distribution with zero mean and some dispersion. The sources that lie 3σ away from the mean are the ones we identify as excess sources (see Figure 2, right). This criteria yields 16 (11% ± 3%) objects with a 3σ detection ($K-[24] > 0.45$ mag) of excess at 24 μm.

We plot the $H\alpha$ EWs versus the excess $K-[24]$ colors in Figure 2. It is clear from Figure 2 that the WTT excess objects do not all lie near some WTTS/CTTS boundary, and the vast majority of these objects have EW($H\alpha$) much lower than 10 Å. Almost all (30 out of 33) CTTSs show 24 μm excess. The exceptions are RX J1150.4-7704, RX J1518.9-4050, and ROX 39. The first two stars would have been WTTSs according to the low-resolution EW($H\alpha$) but are classified as CTTSs because of large $H\alpha$ widths seen in high-resolution spectra. ROX 39 is a K5 star with EW($H\alpha$) = 3.6 Å which is near the WTTSs boundary. Thus, they are relatively weak accretors.

In Figure 3, we plot the [3.6]−[24] color excess against the $K-[24]$ color excess (or EX($K-[24]$)) for the sources that had detections in the involved bands. We note a high degree of correlation between the two excesses and infer that these two measures are consistent with each other. All of the 148 WTTSs with reliable $K-[24]$ colors also have IRAC1 photometry. Of these, 16 (11% ± 3%) had excess detection above the 3σ level, the same as our estimate from $K-[24]$ colors. However, one of the candidate sources from the $K-[24]$ excess objects is not found to be a [3.6]−[24] excess source, and vice versa. This discrepancy is likely due to the fact that there is excess in the IRAC1 band itself. It is easy to see from Figure 3 that the WTTS color excesses have a much wider distribution than the CTTS excesses. Counting only the excess objects, the fraction of CTTS

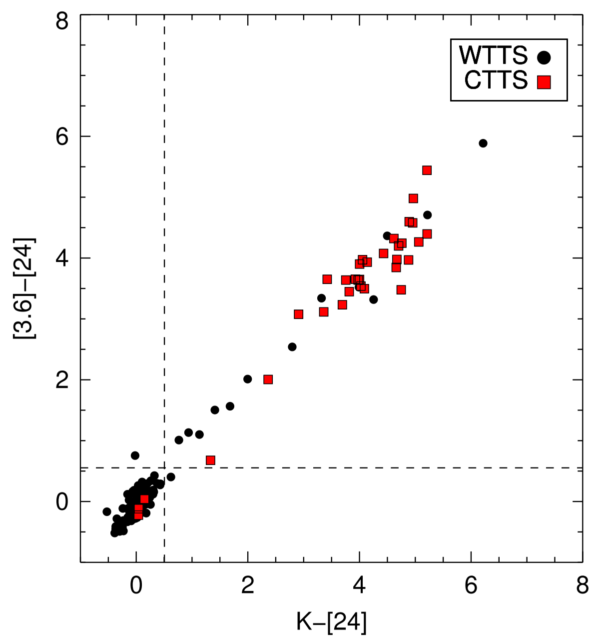

Figure 3. Excess [3.6]−[24] vs. $K-[24]$ colors for our sample. WTTSs are shown as filled circles. CTTSs are shown as squares. The dashed lines are the 3σ markers for excess identification.

(A color version of this figure is available in the online journal.)

with EX($K-[24]$) < 2.5 mag is only 6.7% (2/30). However, 44% ± 16% (7/16) WTTSs excess sources fall in this range. Thus, roughly half of the excess WTTSs fall between CTTSs and diskless stars, in terms of 24 μm excess.

3.1.1. Disk "Turn-on" Wavelengths and Disk Holes

Excess in a particular band indicates the presence of circumstellar dust with temperatures in a certain range. Consideration

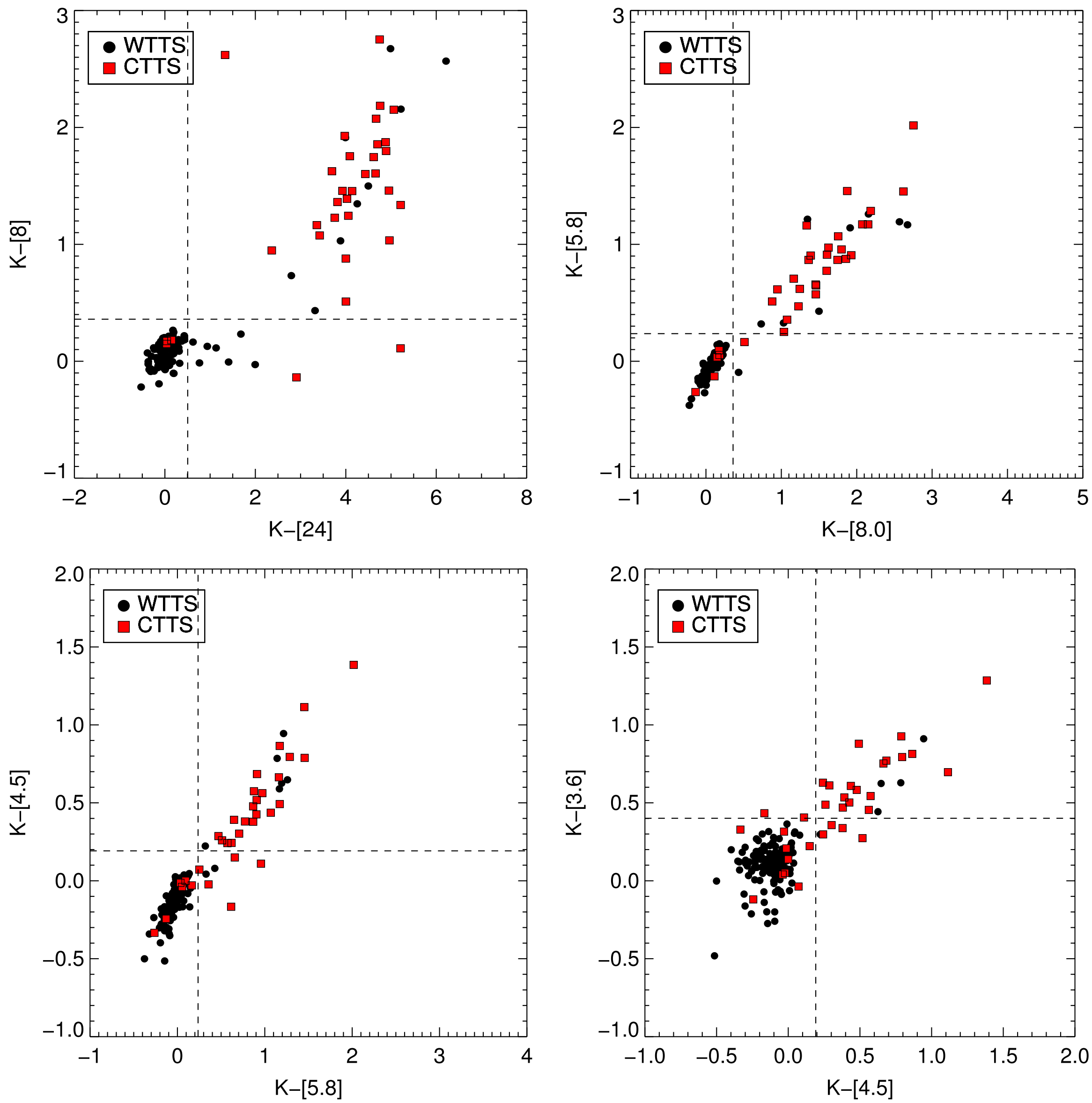

Figure 4. WTTS and CTTS symbols are the same as before. We plot the excess $K-[\mathrm{X}]$ color in adjacent bands against each other, revealing the shortest wavelength band at which the disk emission first "turns on." Here [X] represents the wavelength of the *Spitzer* band. The dashed lines represent the 3σ markers for excess identification.

(A color version of this figure is available in the online journal.)

of the frequency form of Wien's displacement law suggests that these temperatures are roughly 40 K, 120 K, 350 K, 480 K, 620 K, and 780 K for the 70, 24, 8, 5.8, 4.5, and 3.6 μm bands, respectively. For the median stellar luminosity of our sample, 0.5 $L_\odot$, we estimate that these temperatures are reached by circumstellar dust at orbital radii of 100, 10, 1.3, 0.7, 0.4, and 0.25 AU, respectively. When infrared excess in a particular band is accompanied by the lack of excess at shorter wavelengths, an inner cleared region or hole in the circumstellar disk is indicated. We plot the excess in adjacent *Spitzer* bands against each other, in Figure 4, in order to identify the disks with inner holes. We also try to identify the shortest wavelength at which the disk emission first "turns on," i.e., appears above detection limits, as we trace the excess from short to long wavelengths. In the same sense, the disks "turn off" as we go from long to short wavelengths, when their excess emission becomes too small to be detectable.

In the top-right panel of Figure 4, we plot the excess $K-[8.0]$ colors against the $K-[24]$ colors of our sample. There are 7 WTTSs with 24 μm excess that lack 8 μm excess. Thus, 10 disks "turn on" at 24 μm, another one turns on at 8 μm, 2 more turn on at 5.8 μm, and 2 more turn on at 4.5 μm, leaving 4 WTTSs which were already turned on at 3.6 μm and possibly also have excess in the K band. We designate these objects according to their disk "turn-on" wavelengths. Thus, we have 7 **T24** (turns on at 24 μm) objects, 5 **TIRAC** objects (turns on at IRAC wavelengths), and 4 **TNIR** objects (already show excess at IRAC1 and could have K band excess). We will use these designations to describe the SEDs of the objects throughout the paper, and later connect these to plausible physical interpretations of the evolutionary states of the disks. CTTS disks also turn off at IRAC wavelengths, but in fewer numbers than WTTSs. Only one-third of CTTS disks turn off in one of the observed bands, whereas nearly 80% of WTTS disks are observed to turn off.

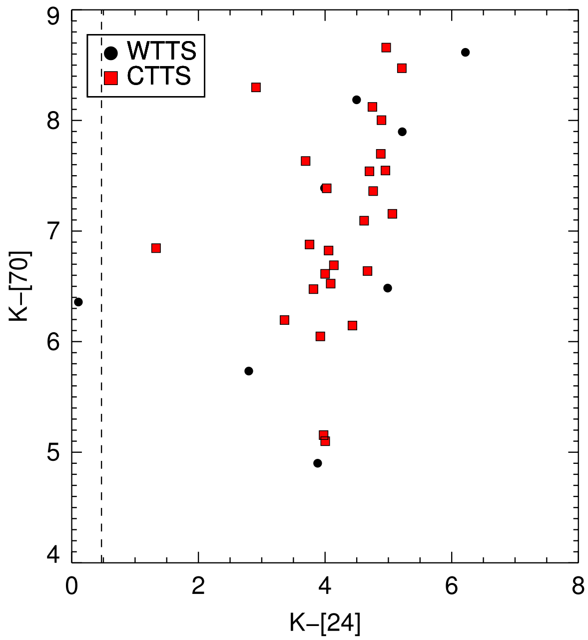

Figure 5. $K-[70]$ excess color vs. $K-[24]$ excess color for our sample. The dashed line is the 3σ marker for 24 μm excess identification.

(A color version of this figure is available in the online journal.)

In Figure 5, we compare infrared excesses at 24 and 70 μm. We see that the 70 μm excess has to be roughly 40 times (i.e., 4 mag) greater than the photosphere to be detected. The 3σ 70 μm sensitivity for our survey is roughly 10 mJy (see Table 2). We detect 8 WTTSs and 27 CTTSs at 70 μm and all of these are detections of excess at least 3.5 mag brighter than the photosphere. Our 70 μm excess detection rate for WTTSs is 5% ± 2%, while for CTTSs it is 82% ± 16%. We find only 1 WTTS with 70 μm excess for which we detect no 24 μm excess. This hardly changes the overall excess rate for WTTSs of 11% ± 3% (17 of 148). This WTTS is HBC 422, a companion to another WTTS, about 35″ away, HBC 423 which itself has a 70 μm excess. If the excess is truly associated with the star, then this indicates cool dust in orbit relatively far from the star (∼50 AU). To keep track of the SED designations we call this a **T70** object since its excess turns on at 70 μm. The disk is very likely optically thin. None of the CTT SEDs show evidence of such large inner holes.

In summary, while ∼89% of WTTSs are diskless, the rest have a rich variety of SEDs, indicating a wide range of evolutionary states. If circumstellar disks progressively clear from the inside out, the SED types ordered from least to most evolved would be **TNIR**, **TIRAC**, **T24**, and **T70**. We designate diskless objects as **RJ** indicating that their SEDs have a Rayleigh–Jeans slope longward of the K band.

3.2. Properties of On-cloud and Off-cloud Sources

The discrepancy in the WTTS excess fractions found in the earlier papers in this series (∼20% in Cieza et al. 2007 and ∼6% in Padgett et al. 2006) strongly suggested that the distance from the cloud may be an important factor affecting the excess rate. It is likely that WTTSs with larger separations from the clouds include a much older population of stars than the ones close to the clouds. To investigate this connection, we attempted to find the projected separations of our sample from their parent clouds in a systematic manner. We defined the cloud edge as the $A_V = 3$ contour line. However, extinction maps produced in the same fashion for all the clouds were not available, especially not for regions a few degrees away from clouds. Thus, we decided to use the dust temperature derived all-sky extinction maps created by Schlegel et al. (1998). These maps were created from COBE/DIRBE and IRAS/ISSA maps and have the calibration quality of the former with the spatial resolution of the latter. The maps show a great deal of filamentary structure and trace the H I maps well but are less reliable in regions where H I is saturated. In comparison to more ideally produced extinction maps, as in Cambrésy (1999), we find that the agreement of the contour lines are at the 10′ level. We should note that, while in cold regions these maps may give reliable extinctions, where there is heating by nearby hot stars as in the case of Ophiuchus, the maps become suspect. From the analysis that follows, however, we will see that we have sufficient accuracy to obtain meaningful results.

Plotting the projected distances (r_c) of the WTTSs estimated from these extinction maps against their $K-[24]$ excess colors, we find that of the 70 WTTSs within 1° of their parent cloud, 13 (19% ± 5%) have disks (Figure 6). Regions within 1° of the cloud edge will be called "on-cloud" hereafter. The excess rate for the 78 WTTSs that lie farther away is 5% ± 3%, i.e., 4 WTTS disks are clearly off-cloud. Given the significant discrepancy between on-cloud and off-cloud excess rates, it seems likely that the off-cloud WTTSs are a physically different group of objects, perhaps older. Moreover, we should remember that the 70 WTTSs which are projected within 1° of the clouds still have some foreground off-cloud objects, so the actual on-cloud excess rate could be much higher than we estimate here.

In the right panel of Figure 6, we display the $K-[24]$ excess colors of each of our targeted WTTS clouds separately. We find excess fractions of 8% ± 6%, 7% ± 4%, 19% ± 7%, and 11% ± 5% for the Chamaeleon, Lupus, Ophiuchus, and Taurus regions, respectively. In terms of the distribution of the different kinds of WTTS disks, all the clouds are quite similar, although we should note it is difficult to draw distinctions from so few detections. Only Ophiuchus has a notably higher WTTS disk fraction, while the rest of the clouds have virtually indistinguishable fractions given the large uncertainties. An offset proportional to the projected separation of WTTSs from their parent clouds has been added to the x-axis values in Figure 6 (right). We note that the off-cloud WTTSs objects with excess are two **TNIR** disks near Chamaeleon and two **T24** disks near Lupus.

The WTTSs with excess in Taurus and Ophiuchus are all within 1° of their cloud edge, while all the Chamaeleon excess sources lie off-cloud (Figure 8). In the literature the mean ages for Taurus and Ophiuchus are often found to be younger than the other two clouds (Allers et al. 2007).

In Figure 7, the A_Vs derived from $J-K$ colors are plotted against the projected distances from the respective clouds. Apart from one clear outlier (T Cha, an optically thick disk) with an $A_V \sim 10$, roughly 1.5 deg from the cloud edge, we see that all high A_V objects lie within 1° of the cloud edge and the highest A_V sources lie well within. T Cha is thought to have a close to edge-on disk (Alcala et al. 1993; Brown et al. 2007) and so in this case the high extinction is probably caused by disk occultation. Almost all the other off cloud sources have low extinctions. This suggests that both A_V and distance from cloud edge has been derived with high fidelity and, moreover, the high A_V sources are very likely embedded in the clouds, and thus real cloud members. The excess rate for WTTSs with $A_V > 1$ is 11 out of 41 (27% ± 8%). Objects with less than zero projected cloud separations (these are within the cloud boundaries) have

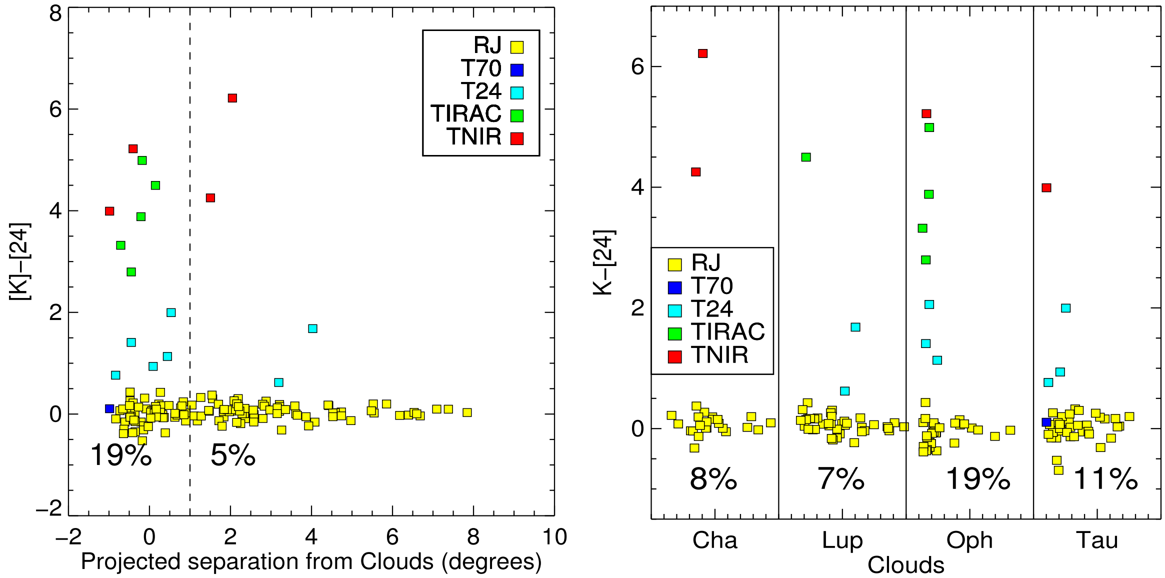

Figure 6. Left: excess $K-[24]$ color vs. distance from cloud edge in degrees. Objects are colored according to their disk "turn-on" wavelengths. **RJ** indicates diskless objects. The dashed line is the 1° from cloud edge demarcation. The excess fractions on either side of this boundary is given at the bottom of the plot. Right: the excess $K-[24]$ color of the WTTS shown for each cloud separately. A small offset proportional to the projected separation from the parent cloud has been added in the horizontal direction for ease of viewing.

(A color version of this figure is available in the online journal.)

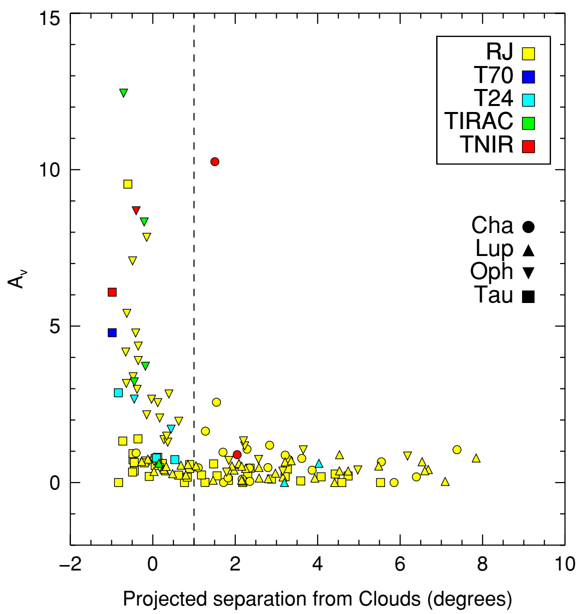

Figure 7. A_V derived from $J-K$ color plotted against projected distance from cloud edge. Negative projected distances indicate objects inside the clouds. Objects are colored according to SED types and are given symbols according to parent cloud region. As expected almost all high extinction objects are on-cloud, while almost all off-cloud objects have low extinctions.

(A color version of this figure is available in the online journal.)

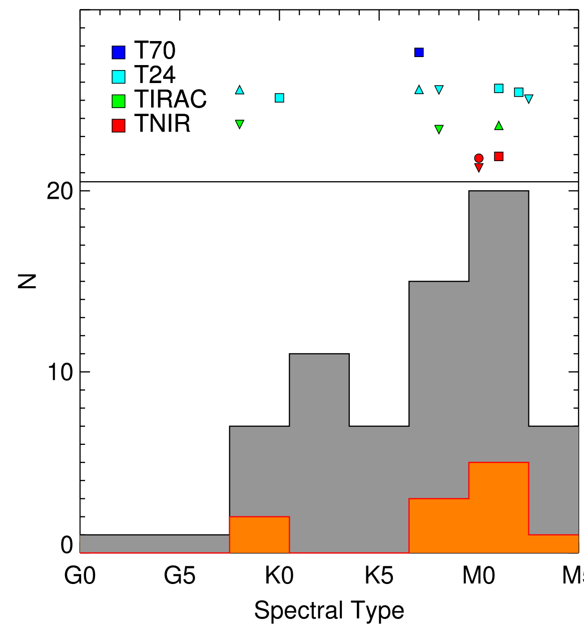

Figure 8. Histogram of the spectral types of WTTSs with $r_c < 1°$ is shown in gray. The histogram of the subset with disks is shown in orange. A very small minority of WTTSs with spectral types earlier than G0 are not shown. Also overlaid on this plot are the symbols representing the types of the individual WTTSs disks. The shapes of the symbols represent different clouds, same as in Figure 7. The excess rate for WTTSs between G0 and K5 is 2/20 (10% ± 7%), while the excess rate for WTTSs between K6 and M5 is 9/46 (20% ± 7%). The significance of the difference in these rates is only about 1σ.

(A color version of this figure is available in the online journal.)

extinctions spanning the entire range starting from zero. Thus, these objects constitute both foreground and cloud-embedded objects.

Since the on-cloud WTTSs are a younger population with much lower contamination by older objects, we investigate the excess rate of these objects with respect to spectral type. In Figure 8, we plot the histogram of the spectral types of WTTSs with $r_c < 1°$ with and without disks. We leave out a few very early type objects because of very low number statistics at that end. The excess rate for spectral types G0 through K5 was 2 of 20 (10% ± 7%), while the excess rate for spectral types K6 through M5 was 9 of 46 (19% ± 7%). The later spectral types seem to have a higher excess rate, but the result is only 1σ significant. However, we see from the disk type designations of the WTTSs in Figure 8 that the less evolved SEDs seems to be concentrated in the later spectral types.

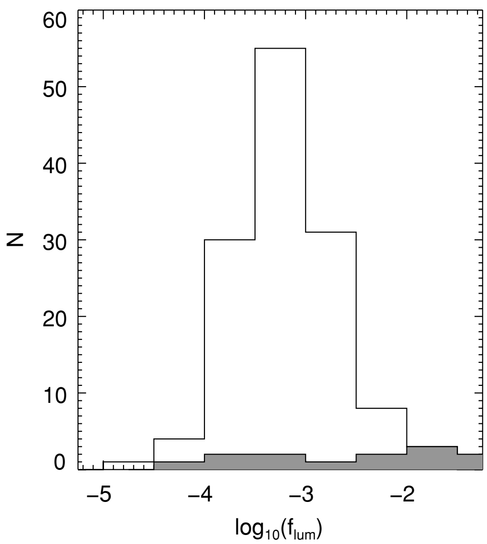

Figure 9. Filled histogram shows the distribution of the measured fractional luminosities ($f_{\rm lum}$) for our WTTSs. The unfilled histogram shows the distribution of the upper limits to $f_{\rm lum}$s for the WTTSs without detections of infrared excess.

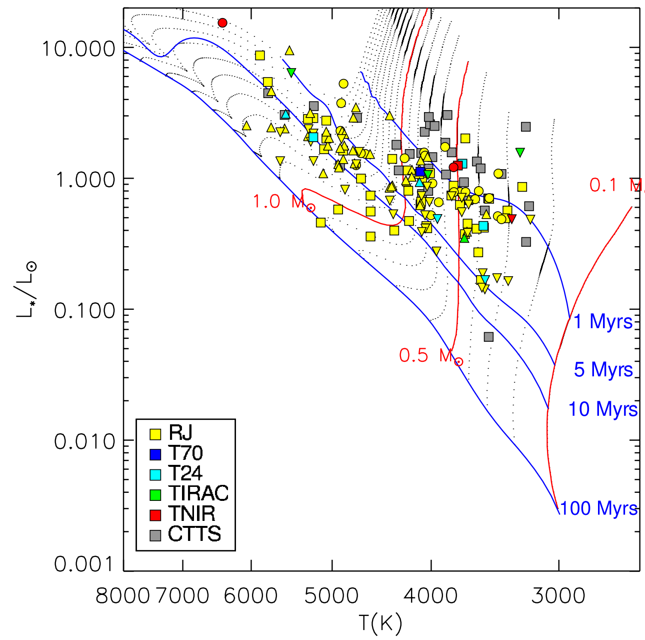

Figure 10. H-R diagram for our sample of stars with the Siess et al. (2000) evolutionary tracks. The solid blue lines are isochrones for 1, 5, 10, and 100 Myr. The 100 Myr line basically coincides with the main-sequence track (not shown here). The solid red lines represent mass tracks for 0.1, 0.5, and 1.0 $M_\odot$, as labeled in the figure.

(A color version of this figure is available in the online journal.)

4. DISCUSSION

4.1. Disk Fractional Luminosities

The fractional luminosities of disks ($f_{\rm lum} = L_{\rm disk}/L_*$) provide a model independent measure of the dust contents of the circumstellar environments. It is also a convenient way to characterize the rich variety of SEDs found around WTTSs by a single number, which is expected to have some connection to their evolutionary status. We compute the fractional luminosities in the following way. We consider only the photometry and upper limits in the IRAC and MIPS bands, since excesses were only computable past the K band. The appropriate photospheric fluxes are subtracted from the *Spitzer* photometry of each star, assuming that the K band fluxes come solely from the photosphere. The flux densities are integrated according to Simpson's rule from the K band through 70 μm. The stellar flux density is similarly integrated from 0.01 μm to 100 μm assuming a blackbody spectrum with the star's temperature, normalized to the K band flux. Thus, $f_{\rm lum}$ is computed by taking the ratio of these two integrals.

However, most of the time, we have only a 70 μm upper limit and/or no 24 μm detection of excess. Thus, there are three cases which we treat separately. For case 1, when we have detections of excess in both MIPS bands, we compute the minimum $f_{\rm lum}$. Past 70 μm, we assume a modified blackbody ($T = 40$ K) where the flux density behaves as $f_\nu \sim \lambda^{-3}$, instead of $f_\nu \sim \lambda^{-2}$ (Rayleigh–Jeans slope). For case 2, when we have a 24 μm excess detection but only a 70 μm upper limit, we use a modified blackbody ($T = 150$ K) past 24 μm. In a few cases where the modified blackbody extrapolates to fluxes above the 70 μm upper limit, the upper limit is adopted as the flux estimate and used as the starting extrapolation point for the modified blackbody. Thus for case 2, we are also computing minimum $f_{\rm lum}$. For case 3, we have no detections of excess in any of the bands, thus we can only compute an upper limit to the $f_{\rm lum}$. This is done by adopting a modified blackbody, which passes through both 24 and 70 μm upper limits. Our estimates for the disk $f_{\rm lum}$ are given in Table 1. It seems that the median sensitivity limit for the WTTS sample is $f_{\rm lum} < 5 \times 10^{-4}$. We also note that we are not sensitive to disks cooler than 40 K. Most of the detected disks have $f_{\rm lum}$ ranging from 5×10^{-2} to 5×10^{-4}, although there are disks which are as tenuous as $f_{\rm lum} \sim 1 \times 10^{-5}$. A histogram of the measured $f_{\rm lum}$ is shown in Figure 9.

The most robust debris disks have $f_{\rm lum} < 1 \times 10^{-2}$ (HR 4796A, β Pictoris). We have nine WTTSs with smaller $f_{\rm lum}$, making them the youngest debris disk candidates. However, we do not know whether these excess emissions results from remnants of primordial disks or second generation disks created by collisional grinding of planetesimals. Only two of these nine debris disk candidates lie beyond 1° of the cloud edge. Moreover, the robust mean age (explained in the next section) of the 9 WTTSs is 1.5 ± 0.4 Myr, with a spread of 1.2 Myr, which makes them as young as the on-cloud WTTS population. Seven of these are **T24** objects, one is a **T70**, and the other one is a **TIRAC** object. Thus, as expected, lower $f_{\rm lum}$ correlate very well with long "turn-on" wavelengths.

4.2. Age Analysis

It is interesting to compare the ages of the WTTSs to the evolutionary states inferred from their disk SEDs. Age analysis is always a difficult task since evolutionary tracks are often extremely close together on the Hertzsprung–Russell (H-R) diagram. According to the stellar evolutionary tracks of Siess et al. (2000), all the mass tracks are in a very narrow temperature range at 1 Myr (3000–4500 K; see Figure 10). For our sample, we have an additional difficulty in estimating ages. The distances to the individual objects, especially the ones located outside the clouds, are not known precisely and should be assumed to be uncertain by ∼20%. This introduces a 40% uncertainty into the intrinsic luminosity of the object, dominating any calibration or bolometric correction uncertainty in the age determination. Moreover, there is the uncertainty in temperature which is assumed to be a spectral subtype. However, these problems are somewhat mitigated by the fact that, for low mass stars, luminosities can decrease by a factor of 6 as the star ages from 1 to 10 Myr. Moreover, when analyzing the properties of an ensemble, the median ages of the various classes of objects are less disturbed than the individual ages due to the present uncertainties. Large variations in the mean ages of two classes of objects may still be discernible.

As shown by Cieza et al. (2007), even though absolute ages can vary significantly depending on which evolutionary models are used, the relative ages between objects are quite reliable. Our age estimates, all of which come from the Siess et al. (2000) models, should only be used to compare the relative ages of groups of objects.

We assume that each star in our sample is at the distance of their parent cloud which we take from the literature: 180 pc for Chamaeleon II, 200 pc for Lupus, 125 pc for Ophiuchus, and 145 pc for Taurus(de Geus et al. 1989; Whittet et al. 1997; Wichmann et al. 1998; Comerón 2008). These distances are used to obtain the absolute K magnitudes from the extinction corrected apparent K magnitudes. The intrinsic luminosities were computed from bolometric corrections applied to the absolute K magnitudes. Bolometric corrections to the K magnitudes were derived from a table presented in Kenyon & Hartmann (1995). The intrinsic luminosities and the stellar spectral types are then used to estimate the stellar ages, using the Siess et al. (2000) evolutionary models. In Figure 10, we place our objects on an H-R diagram. The error bars in the intrinsic luminosities and the temperatures discussed above are not shown in the figure. Plotting these large errors bars on an already complex plot would only serve to muddle the subtle separations between different groups of objects.

In the following analysis, we quote the robust means of the ages of various groups of stars. This quantity is measured by taking the median and the robust sigma of a group of objects. The robust sigma is calculated using the IDL routine, *robust_sigma.pro*. All values that lie 3σ (robust) away from the median are rejected. The mean of the rest of the values is then calculated along with the uncertainty in this mean. The percentage of rejected values is never more than 20%.

The first thing to notice in Figure 10, is that most CTTSs are younger than 1 Myr (61% or 20/33). All of them are younger than 10 Myr, with just one exception. For the WTTSs, only 16% (22/148) are younger than 1 Myr. For the WTTSs younger than 1 Myr, 41% $\pm$ 14% (9/22) have disks, while only 6% $\pm$ 2% (8/126) WTTSs older than 1 Myr have disks. We can also look at the robust mean ages of CTTSs, WTTSs with disks, and WTTSs without disks which are 0.8 $\pm$ 0.1, 1.3 $\pm$ 0.3, and 3.7 $\pm$ 0.3 Myr, respectively.

There is a strong trend in overall excess fraction with age. In the three age bins, $t < 1$ Myr, 5 Myr $> t >$ 1 Myr, and $t >$ 5 Myr, the excess fractions were 45% $\pm$ 14%, 8% $\pm$ 3%, and 4% $\pm$ 3% of WTTSs, respectively. Furthermore, the mean ages of each evolutionary group of SEDs show a progressive trend. The robust means of the ages of **TNIR**, **TIRAC**, **T24**, and diskless objects are 0.6 $\pm$ 0.1, 1.3 $\pm$ 0.3, 1.5 $\pm$ 0.4, and 4.1 $\pm$ 0.2 Myr, respectively. The robust mean ages of on-cloud and off-cloud WTTSs are 2.3 $\pm$ 0.2 and 4.2 $\pm$ 0.4 Myr, respectively. Of course, the individual ages have very large uncertainties and depend on which evolutionary model is used to estimate them (Cieza et al. 2007; Baraffe et al. 2009). However, the robust mean ages of each group of stars, especially their relative ages, are clearly less affected by these uncertainties.

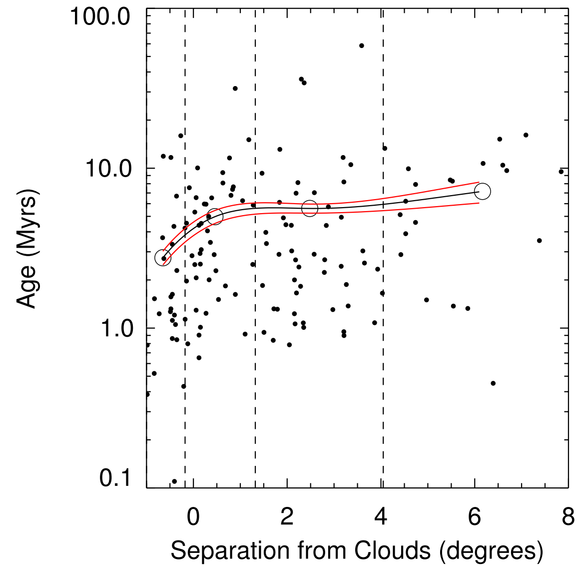

Figure 11. Ages obtained from the Siess et al. (2000) evolutionary tracks vs. the projected separations of the WTTSs from their parent cloud. The vertical dashed lines demarcate four cloud-separation bins within which mean ages are calculated. The solid black curve is a spline fit through these mean ages. The red curves indicate the 1σ errors in the mean ages. Thus, the mean age of objects increases noticeably with increasing separation from the cloud boundaries.

(A color version of this figure is available in the online journal.)

It is difficult to reason that the on-cloud and off-cloud WTTS populations, which are only 2 Myr apart but very well mixed in age, could have such different disk fractions (20% for on-cloud, 5% for off-cloud). The disk fraction would be much closer if the ages were really that mixed. We propose that the disk fractions are actually very sensitive to age, and the vast majority of disks evolve into the tenuous end phase of the primordial disk by roughly 3.5 Myr. It is quite plausible that the ages are actually a strong function of separation from the cloud, but that this relationship is confused by the uncertainty in the distances. We investigate this scenario in Figure 11, where we plot the measured ages versus the projected separations. We see that the mean ages in the four bins increase gradually with separation, and the errors in the means are small enough to make this trend significant. At projected cloud separations of -0.65, 0.46, 2.5, and 6.2 deg, the mean ages are 2.75 $\pm$ 0.5, 5 $\pm$ 0.75, 5.6 $\pm$ 0.8, and 7.2 $\pm$ 1.6 Myr. Of course, an age–separation relation is not expected to be strict as there many other factors involved in the spatial distribution of young stars.

4.3. Connection Between Disk Fraction and Multiplicity

Since even extremely young WTTSs have a measurably lower disk fraction than CTTSs, it has been conjectured that unseen stellar companions may be responsible for clearing the inner disks of WTTSs. The alternative explanations are that WTTSs are slightly older objects or that they resulted from very different initial conditions than CTTSs, which make them more susceptible to disk dissipation by photo-evaporation or tidal interaction, for example. Nevertheless, we look at published multiplicity studies on our objects, to see if binaries show measurably different disk fractions. Also of interest is whether binary systems halt disk accretion quickly. In other words, are WTTSs preferentially binaries?

The most comprehensive study to date on the effect of binarity on the disk excess rate is that of Cieza et al. (2009). They found that the IRAC excess fraction for binaries with separation less

Table 4
Average Properties of Different SED Object Types

Statistics	TNIR	TIRAC	T24	RJ
N	24	13	9	134
Mean age (Myr)	0.6 ± 0.1	1.3 ± 0.3	1.5 ± 0.4	4.1 ± 0.2
Mean $f_{\rm lum}$	$7 \pm 0.7 \times 10^{-2}$	$3.7 \pm 0.7 \times 10^{-2}$	$1.7 \pm 0.5 \times 10^{-3}$	$<5 \pm 1 \times 10^{-4}$

40 AU is 38% ± 6%, while it was 78% ± 7% for systems with larger separation. However, their study pertains to inner hole clearing sizes of ∼1 AU and somewhat younger objects, since their sample was composed of mostly on-cloud objects and they only dealt with the IRAC bands.

The multiplicity information on our sample comes from several kinds of companion surveys. Apart from the Cieza et al. (2009) compilation of speckle interferometry, radial velocity, lunar occultation, and adaptive optics surveys, we found other binarity information in the literature which are listed in Table 1. To summarize the disparate kinds of companion searches, these surveys can find or rule out the existence of a companion at two regimes. The spectroscopic surveys are sensitive to systems with periods of hundreds of days (roughly 1 AU separation) and the imaging surveys are sensitive to companions with roughly 0″.15 separation (∼20 AU). We count as binary all objects for which any kind of companion was found within 1″. All objects which were unsuccessfully searched we consider single. Systems with widely separated companions (hundreds of AU) can easily harbor a disk around either component, as the companion only forces disk truncation to one third the total separation (Papaloizou & Pringle 1977).

In our sample of 33 CTTSs, the ratio of the number of CTTSs for which companions were found versus the total number searched is 9/19 (47% ± 16%). The same ratio for the WTTSs is 27/82 (33% ± 6%). Despite the small number of sources, there is no evidence in these data that WTTSs are more likely than CTTSs to be binaries.

Now, 7 of the 31 (23% ± 4%) binary WTTSs exhibit IR excess, whereas 6 of 55 (11% ± 4%) purportedly single WTTSs show IR excess. Since binaries stars have two chances to have a disk, the disk fraction of an individual star in a binary system is $\mathrm{DF}_i = 1 - \sqrt{1 - \mathrm{DF}_s}$, where DF_s is the disk fraction of the system, which is all we can measure for unresolved pair (Cieza et al. 2009). Thus, our individual WTTS disk fraction turns out be 12% ± 3%, virtually the same as the single star disk fraction. However, our WTTS binaries include systems with wide separations (∼100 AU) which are expected to be much more conducive to disks. We also included old WTTSs which are likely to have lower disk fractions. A combination of population contamination and biases is probably masking the effect of binarity on disk lifetimes as seen by Cieza et al. (2009).

When we try to divide our sample into the two groups chosen by Cieza et al. (2009), we find that we have very small statistics. In the first WTTS group we place all the spectroscopic binaries, and the detected binaries with separation less than 0″.2 (roughly $\rho < 40$ AU), while in the second WTTS group, we put all the wider binaries. For the tight binaries, we get an excess fraction of 4/17 (24% ± 12%), while the wide binary disk fraction is 3/14 (21% ± 12%). Thus, the results are inconclusive. If a study complementary to the Cieza et al. (2009) work were to be done for older WTTSs and for disks detected as MIPS excess, we would need a much larger sample of off-cloud binaries.

Recent studies which have compared disk fractions in single and binary systems show how different results are obtained from different samples. Pascucci et al. (2008) found no evidence of the effect of binarity on disk emission in a carefully selected medium-separation sample ($\rho \sim$ 14–420 AU) in Taurus (age ∼1–3 yr). However, for the late-type stars in the 8 Myr old η Chamaeleontis cluster, Bouwman et al. (2006) found that 8 of 9 single stars and 1 of 6 binary systems ($\rho < 20$ AU) had a disk. Although these results seem to show that small separation systems affect disk lifetimes while large separation systems do not, the two samples have different ages. Differing ages, separations, masses, and viewing angles of the systems under study, which are often quite uncertain, can easily confuse the true effect of binarity in small samples. Pott et al. (2010) showed that there are no stellar companions in five of the most clearly classifiable transition disks, in the region between ∼0.35 and 4 AU from the stars. Thus, if one has to invoke companions as an explanation for the disk clearings, they would have to be substellar.

4.4. Physical Interpretation of SEDs

The objects with SED types **TNIR**, **TIRAC**, **T24**, **and RJ** had mean ages of 0.6 ± 0.1, 1.3 ± 0.3, 1.5 ± 0.4, and 4.1 ± 0.2 Myr and mean disk fractional luminosities of these groups were $(7 \pm 0.7) \times 10^{-2}$, $(3.7 \pm 0.7) \times 10^{-2}$, $(1.7 \pm 0.5) \times 10^{-3}$, $(3.8 \pm 1) \times 10^{-3}$, and lastly a mean upper limit of $(5 \pm 1) \times 10^{-4}$, respectively. Thus, in terms of age and disk fractional luminosity these statistics strongly suggest an evolutionary trend through these SED types. The average properties of the objects of different SED types are shown in Table 4.

The **T24** objects have comparable $f_{\rm lum}$ to known resolved debris disks, and are probably optically thin disks with inner clearings no larger than the terrestrial planet regions. About 6% ± 4% of accreting stars (CTTSs) have SEDs of this type. The **TIRAC** objects are just a little younger, with smaller inner clearings and larger fractional luminosities which are just above the informal debris disk demarcation line at $f_{\rm lum} = 1 \times 10^{-2}$. About 24% ± 9% of accreting stars have SEDs of this type. The **TNIR** disks fall into the category of traditional optically thick disks (61% ± 14% of CTTSs fall into this category). It should be noted that although we have designated the **RJ** objects as diskless they might easily have debris disk of fractional luminosity comparable to the β Pictoris disk in regions analogous to their Kuiper belts.

In Figure 12, we examine the SEDs of these groups of objects. The shapes of the SEDs of most of the WTTS **TNIR** and **TIRAC** objects indicate a depleted region or a gap in the disks. The excess in the IRAC bands definitely indicate an inner disk ($r \sim$ 1 AU), but the emission coming from the middle disk ($r \sim$ 40 AU) is obviously much more robust as seen in the MIPS bands. Thus, it seems that the middle disk survives the inner disk. Cieza et al. (2008) found that objects with low 24 μm excesses are not detected in the submillimeter, just as we found that these objects are also not detected at 70 μm. They understood this to indicate that the inner disk only dissipates after the outer disk has been significantly depleted of mass.

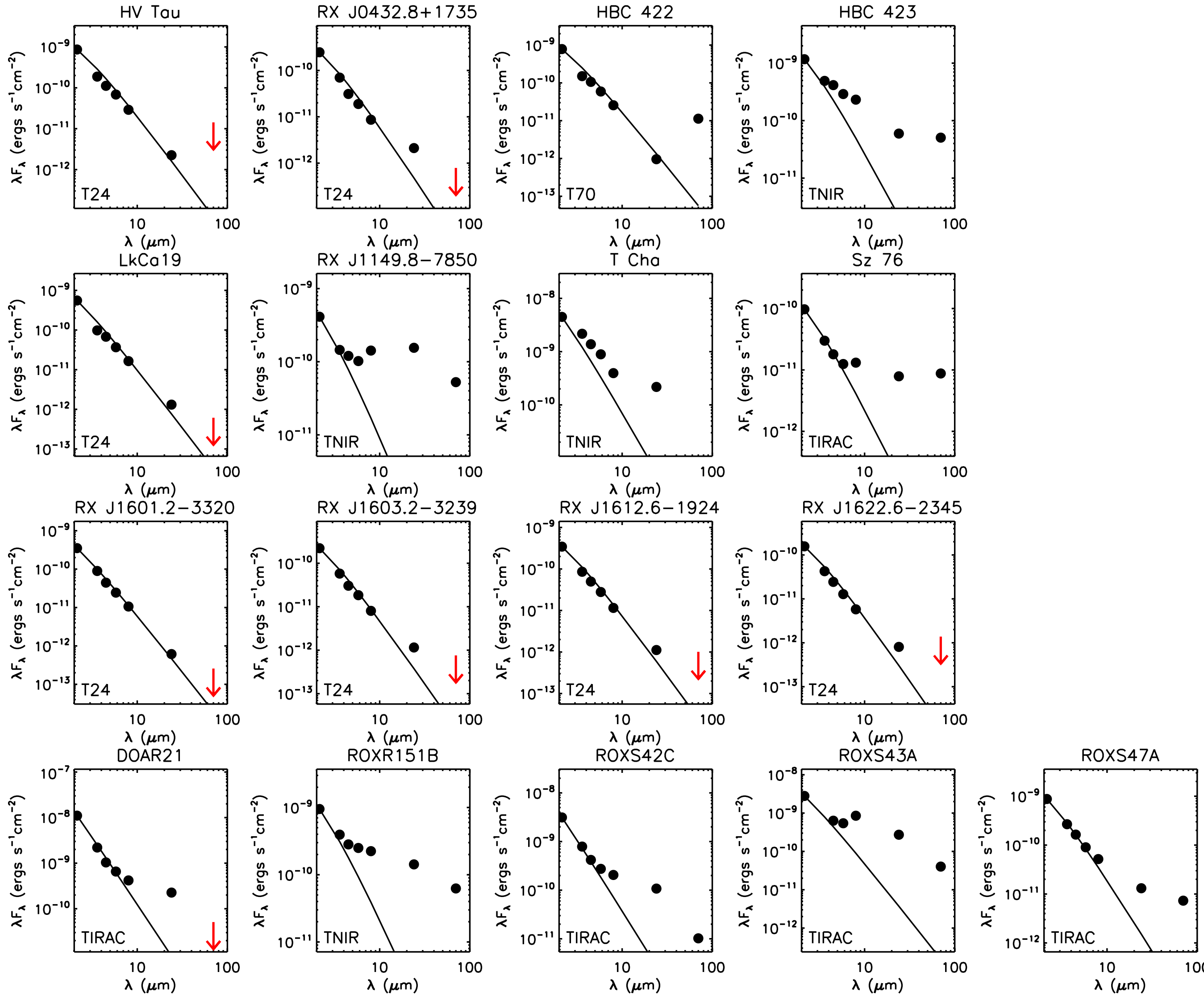

Figure 12. SEDs of the WTTSs with excess. The solid line represents the Planck function of the appropriate temperature normalized to the extinction corrected *K*-band flux. The red arrows are 3σ upper limits to the 70 μm flux density. The plots are labeled with their disk "turn-on" classifications which are also given in Table 1.

(A color version of this figure is available in the online journal.)

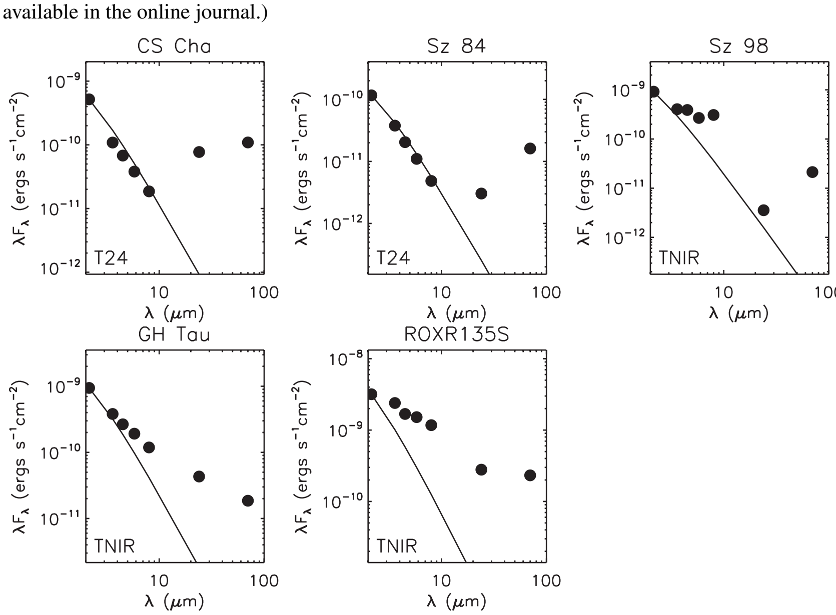

Figure 13. SEDs of the interesting CTTSs with excess (see Section 4.5). The solid line represents the Planck function of the appropriate temperature normalized to the extinction corrected *K*-band flux. The plots are also labeled with their disk "turn-on" classifications which are also given in Table 1.

4.5. New Interesting Objects

Accreting disks with large holes. CS Cha and Sz 84 fall into this category of objects. Was it grain growth that cleared out the dust? Are they accreting because there is no inner companion to stop the gas flow or are they accreting despite an inner companion? They show no excess in the IRAC bands but show robust excesses at 24 and 70 μm (Figure 13). They both have disks with fractional luminosities of $\sim$0.1, and they are both solid accretors with FW.1H($H\alpha$) of $\sim$400 km s^{-1}. CS Cha has a companion (mass $\sim$ 0.1 $M_\odot$; Guenther et al. 2007) with a 2435 day period ($\rho \sim$ 3 AU), while Sz 84 was not targeted in a high-resolution search. The CS Cha SED from earlier *Spitzer* photometry and IRS spectra has been modeled as disk emission in detail to predict a 43 AU inner hole (Espaillat et al. 2007). Given the IRAC and MIPS photometry we obtained, both disks can be modeled with holes at small as 2 AU.

WTTSs with robust disks. There are four stars of this type: HBC 423, RX J1149.8-7850, T Cha, and ROXR1 51b (Figure 12). All these show robust emission at 24 and 70 μm. The IRAC fluxes of these objects clearly show very depleted inner regions. These objects represent the youngest non-accreting or weakly accreting disks. Why has accretion weakened? How is the disk maintained?

Zodiacal dust disks. The CTTSs Sz 98 exhibits excess emission which basically has a Rayleigh–Jeans slope beyond 6 μm and peaks near the IRAC2 band (Figure 13). This indicates a warm contributor to the excess ($T \sim 600$ K), such as would be expected from a dust ring confined to within 0.5 AU of the star. The 8 μm flux is actually anomalously high and inconsistent with the 24 μm detection unless it results from some line emission (e.g., from silicates or PAHs). Sz 98 is of spectral type K8 and is known to be a spectroscopic single, though it may have a companion at separations between 0$''$.1 and 1$''$.

Intermediate separation binaries with robust disks. Binaries at a few tens of AU separations are supposed to make the least conducive environments for massive circumstellar disks. If their physical separations are a few tens of AU, then these objects are interesting because they provide test cases to current theories of planet formation in binary systems (Quintana & Lissauer 2006; Marzari & Barbieri 2007). Binary systems with projected separations between 0$''$.1 and 0$''$.4 ($\rho \sim$ 15 to 60 AU) with fractional disk luminosities above 0.01 are WTTSs, HBC 423 (**TNIR**), and ROXS 42C (**TIRAC**; Figure 12) and CTTSs, GH Tau (**TNIR**), and ROXR1 135S (**TNIR**; Figure 13). All of these show robust 70 μm emission which is either rising or roughly flat with respect to their 24 μm fluxes. The SEDs show no signs of gaps in the disk. These systems may thus be pointing to non-disruptive mechanisms for companion and disk interactions that we may not have foreseen.

5. CONCLUSIONS

We have presented the final results of the first large scale far infrared disk survey of WTTSs. The WTTS stars in the young star-forming regions within 200 pc (Chamaeleon, Lupus, Ophiuchus and Taurus) were probed for infrared excess from 3.6 to 70 μm, in an effort to study the evolutionary status of their disks. We showed that overall 11% of WTTSs have a disk brighter than the β Pictoris debris disk ($f_{\rm lum} = 2 \times 10^{-3}$). However, the disk fraction for WTTSs within 1° of the nearest cloud was 19%, while the disk fraction for WTTSs farther away was 5%. As we move from on-cloud to off-cloud, stars get gradually older and have progressively lower disk fractions.

Of the fraction detected with disks, objects were classified into five groups according to disk "turn-on" wavelengths **TNIR**, **TIRAC**, **T24**, **T70**, **and RJ**. These groups showed easily identifiable trends in terms of age and fractional luminosity. They suggest a sequential transition of accreting optically thick disks into passive optically thick disks into optically thin disks and eventually into apparently diskless systems with $f_{\rm lum} < 5 \times 10^{-4}$ over roughly 4 Myr. Even though the timescales for individual objects may vary wildly, objects with more evolved SEDs on average tend to be older. The incidence rate of β Pictoris-like debris disks for both the on and off-cloud WTTSs may be much higher than the disk rate reported here, since fainter disks are just beyond the capability of our survey.

The mean ages of the CTTSs, and on-cloud and off-cloud WTTSs were also distinguishable from each other because of large statistics in each of these groups. The on-cloud WTTSs seem be measurably older than CTTSs (mean age $\sim$0.8 $\pm$ 0.1 Myr), but they still constitute a very young population (mean age $\sim$2.3 $\pm$ 0.3 Myr). One reason why previous studies have not reported this difference is perhaps because even our on-cloud WTTSs include some older stars, due to a bias in the *ROSAT* selection. However, the mean age of WTTSs with disks (1.3 $\pm$ 0.3 Myr) is basically the same as that of the CTTSs, which indicates that systems with disks are a younger group. However, for the off-cloud objects, we may attach a lower age bound of $\sim$3 Myr, while the upper bound remains somewhere around 100 Myr deduced from X-ray and lithium detections. Our analysis, however, suggested that the off-cloud WTTS apparent luminosities are consistent with an age of less than 10 Myr. Thus, they are indeed predominantly an older population as previously surmised (Padgett et al. 2006; Cieza et al. 2007), and the nature of this still arguably young (3–10 Myr old) population remains a very interesting question.

The analysis of the effect of binarity on disk fractions was inconclusive because of the small number of binaries in our sample and the small excess rates we are dealing with. We are thus not able to complement or test the results of Cieza et al. (2009). An interesting study would be to look at the MIPS disk fractions of a sample of off-cloud binary WTTSs numbering in the hundreds, to get beyond the diluting effects of the differing viewing angles, masses and ages of the systems. Such a study would explain the effect of binarity on outer disks in relatively older systems.

When looking at the disk fraction as a function of spectral type, we restricted ourselves only to on-cloud objects, in order to consider only the young objects. The excess rate for spectral types G0 through K5 was 10% $\pm$ 7% while that for later spectral types was 19% $\pm$ 7%. Also it seems that the less evolved SED types are concentrated in the later spectral types.

We also find that, in a large number of cases, nebulosity or confusion with nearby YSOs can result in false detections of 70 μm excess around WTTSs. Such problems can be avoided by careful comparisons of the emission centers at 70 μm and IRAC bands and requiring the shapes of emission to be point source-like. However, since false positives were found to be as frequent as bona fide detections, it seems that the environs of WTTSs within $\sim$ 20$''$ are frequently occupied by young objects or cloud material. Higher resolution far-infrared and submillimeter imaging of the neighboring cold cloud material may reveal heretofore unknown ways in which the WTTS environs affect their disks.

Support for this work, which is part of the *Spitzer* Legacy Science Program, was provided by NASA through contracts

1224608, 1230782, and 1230799 issued by the Jet Propulsion Laboratory, California Institute of Technology under NASA contract 1407. This publication makes use of data products from the Two Micron All Sky Survey, which is a joint project of the University of Massachusetts and the Infrared Processing and Analysis Center funded by NASA and the National Science Foundation. We also acknowledge use of the SIMBAD database.

REFERENCES

Alcala, J. M., Covino, E., Franchini, M., Krautter, J., Terranegra, L., & Wichmann, R. 1993, A&A, 272, 225
Alcalá, J. M., et al. 2008, ApJ, 676, 427
Alexander, R. D., Clarke, C. J., & Pringle, J. E. 2006, MNRAS, 369, 229
Allers, K. N., et al. 2007, ApJ, 657, 511
Andrews, S. M., & Williams, J. P. 2005, ApJ, 631, 1134
Artymowicz, P., & Lubow, S. H. 1994, ApJ, 421, 651
Baraffe, I., Chabrier, G., & Gallardo, J. 2009, ApJ, 702, L27
Barkhatova, K. A., Zakharova, P. E., Shashkina, L. P., & Orekhova, L. K. 1985, SvA, 29, 499
Barrado y Navascués, D., & Martín, E. L. 2003, AJ, 126, 2997
Barsony, M., Koresko, C., & Matthews, K. 2003, ApJ, 591, 1064
Beckwith, S. V. W., Sargent, A. I., Chini, R. S., & Guesten, R. 1990, AJ, 99, 924
Bouwman, J., Lawson, W. A., Dominik, C., Feigelson, E. D., Henning, T., Tielens, A. G. G. M., & Waters, L. B. F. M. 2006, ApJ, 653, L57
Brown, J. M., et al. 2007, ApJ, 664, L107
Cambrésy, L. 1999, A&A, 345, 965
Carpenter, J. M., Mamajek, E. E., Hillenbrand, L. A., & Meyer, M. R. 2006, ApJ, 651, L49
Chapman, N. L., et al. 2007, ApJ, 667, 288
Chen, C. H., Jura, M., Gordon, K. D., & Blaylock, M. 2005, ApJ, 623, 493
Cieza, L. A., Swift, J. J., Mathews, G. S., & Williams, J. P. 2008, ApJ, 686, L115
Cieza, L., et al. 2007, ApJ, 667, 308
Cieza, L. A., et al. 2009, ApJ, 696, L84
Clarke, C. J., Gendrin, A., & Sotomayor, M. 2001, MNRAS, 328, 485
Comerón, F. 2008, in Handbook of Star Forming Regions, Vol. II, ed. B. Reipurth (San Francisco, CA: ASP), 295
Covino, E., Alcala, J. M., Allain, S., Bouvier, J., Terranegra, L., & Krautter, J. 1997, A&A, 328, 187
Currie, T., et al. 2007, ApJ, 659, 599
Dahm, S. E., & Hillenbrand, L. A. 2007, AJ, 133, 2072
de Geus, E. J., de Zeeuw, P. T., & Lub, J. 1989, A&A, 216, 44
Dullemond, C. P., & Dominik, C. 2005, A&A, 434, 971
Espaillat, C., et al. 2007, ApJ, 664, L111
Evans, N. J., II., et al. 2003, PASP, 115, 965
Fazio, G. G., et al. 2004, ApJS, 154, 10
Gautier, T. N., III., et al. 2007, ApJ, 667, 527
Ghez, A. M., McCarthy, D. W., Patience, J. L., & Beck, T. L. 1997, ApJ, 481, 378
Gordon, K. D., et al. 2007, PASP, 119, 1019
Gorlova, N., Balog, Z., Rieke, G. H., Muzerolle, J., Su, K. Y. L., Ivanov, V. D., & Young, E. T. 2007, ApJ, 670, 516
Gorlova, N., Rieke, G. H., Muzerolle, J., Stauffer, J. R., Siegler, N., Young, E. T., & Stansberry, J. H. 2006, ApJ, 649, 1028
Gras-Velázquez, À., & Ray, T. P. 2005, A&A, 443, 541
Guenther, E. W., Esposito, M., Mundt, R., Covino, E., Alcalá, J. M., Cusano, F., & Stecklum, B. 2007, A&A, 467, 1147
Gutermuth, R. A., Bourke, T., Allen, L., Myers, P., & Gould Belt Legacy Team, 2007, BAAS, 38, 881
Haisch, K. E., Lada, E. A., & Lada, C. J. 2001, ApJ, 553, L153
Hartmann, L., Calvet, N., Gullbring, E., & D'Alessio, P. 1998, ApJ, 495, 385
Hartmann, L., Stauffer, J. R., Kenyon, S. J., & Jones, B. F. 1991, AJ, 101, 1050
Harvey, P. M., et al. 2006, ApJ, 644, 307
Hernández, J., Briceño, C., Calvet, N., Hartmann, L., Muzerolle, J., & Quintero, A. 2006, ApJ, 652, 472
Hueso, R., & Guillot, T. 2005, A&A, 442, 703
Indebetouw, R., et al. 2005, ApJ, 619, 931
Jensen, E. L. N., Cohen, D. H., & Gagné, M. 2009, ApJ, 703, 252
Keller, J. R. 2004, MS thesis, Northern Arizona Univ.
Keller, J. R., Koerner, D. W., & C2D SIRTF Legacy Team, 2003, BAAS, 35, 1210
Kenyon, S. J., & Hartmann, L. 1995, ApJS, 101, 117
Köhler, R. 2001, AJ, 122, 3325
Kohler, R., & Leinert, C. 1998, A&A, 331, 977
Lada, C. J., et al. 2006, AJ, 131, 1574
Lafrenière, D., Jayawardhana, R., Brandeker, A., Ahmic, M., & van Kerkwijk, M. H. 2008, ApJ, 683, 844
Leinert, C., Zinnecker, H., Weitzel, N., Christou, J., Ridgway, S. T., Jameson, R., Haas, M., & Lenzen, R. 1993, A&A, 278, 129
Lin, D. N. C., & Papaloizou, J. 1979, MNRAS, 186, 799
Low, F. J., Smith, P. S., Werner, M., Chen, C., Krause, V., Jura, M., & Hines, D. C. 2005, ApJ, 631, 1170
Luhman, K. L., et al. 2008, ApJ, 675, 1375
Martín, E. L. 1998, AJ, 115, 351
Marzari, F., & Barbieri, M. 2007, A&A, 467, 347
Megeath, S. T., Hartmann, L., Luhman, K. L., & Fazio, G. G. 2005, ApJ, 634, L113
Melo, C. H. F. 2003, A&A, 410, 269
Meyer, M. R. 1996, PhD thesis, Max–Planck–Institut für Astronomie, Königstuhl
Meyer, M. R., Backman, D. E., Weinberger, A. J., & Wyatt, M. C. 2007, in Protostars and Planets V, ed. B. Reipurth, D. Jewitt, & K. Keil (Tucson, AZ: Univ. Arizona Press), 573
Muench, A. A., Lada, C. J., Luhman, K. L., Muzerolle, J., & Young, E. 2007, AJ, 134, 411
Osterloh, M., & Beckwith, S. V. W. 1995, ApJ, 439, 288
Padgett, D. L., et al. 2006, ApJ, 645, 1283
Padgett, D. L., et al. 2008, ApJ, 672, 1013
Palla, F., & Stahler, S. W. 2000, ApJ, 540, 255
Papaloizou, J., & Pringle, J. E. 1977, MNRAS, 181, 441
Papovich, C., et al. 2004, ApJS, 154, 70
Pascucci, I., Apai, D., Hardegree-Ullman, E. E., Kim, J. S., Meyer, M. R., & Bouwman, J. 2008, ApJ, 673, 477
Pott, J., Perrin, M. D., Furlan, E., Ghez, A. M., Herbst, T. M., & Metchev, S. 2010, ApJ, 710, 265
Prato, L. 2007, ApJ, 657, 338
Quintana, E. V., & Lissauer, J. J. 2006, Icarus, 185, 1
Ratzka, T., Köhler, R., & Leinert, C. 2005, A&A, 437, 611
Rebull, L. M., et al. 2008, ApJ, 681, 1484
Rieke, G. H., et al. 2005, ApJ, 620, 1010
Rieke, G. H., et al. 2004, ApJS, 154, 25
Sartoretti, P., Brown, R. A., Latham, D. W., & Torres, G. 1998, A&A, 334, 592
Schlegel, D. J., Finkbeiner, D. P., & Davis, M. 1998, ApJ, 500, 525
Sicilia-Aguilar, A., Hartmann, L. W., Fürész, G., Henning, T., Dullemond, C., & Brandner, W. 2006, AJ, 132, 2135
Siegler, N., Muzerolle, J., Young, E. T., Rieke, G. H., Mamajek, E. E., Trilling, D. E., Gorlova, N., & Su, K. Y. L. 2007, ApJ, 654, 580
Siess, L., Dufour, E., & Forestini, M. 2000, A&A, 358, 593
Silverstone, M. D., et al. 2006, ApJ, 639, 1138
Simon, M., et al. 1995, ApJ, 443, 625
Stapelfeldt, K. R., Ménard, F., Watson, A. M., Krist, J. E., Dougados, C., Padgett, D. L., & Brandner, W. 2003, ApJ, 589, 410
Stauffer, J. R., et al. 2005, AJ, 130, 1834
Steffen, A. T., et al. 2001, AJ, 122, 997
Su, K. Y. L., et al. 2006, ApJ, 653, 675
Trilling, D. E., et al. 2008, ApJ, 674, 1086
Trilling, D. E., et al. 2007, ApJ, 658, 1289
White, R. J., & Basri, G. 2003, ApJ, 582, 1109
Whittet, D. C. B., Prusti, T., Franco, G. A. P., Gerakines, P. A., Kilkenny, D., Larson, K. A., & Wesselius, P. R. 1997, A&A, 327, 1194
Wichmann, R., Bastian, U., Krautter, J., Jankovics, I., & Rucinski, S. M. 1998, MNRAS, 301, L39
Wichmann, R., Covino, E., Alcalá, J. M., Krautter, J., Allain, S., & Hauschildt, P. H. 1999, MNRAS, 307, 909
Wichmann, R., et al. 2000, A&A, 359, 181
Young, K. E., et al. 2005, ApJ, 628, 283